ALGORITHM THEORETICAL BASIS DOCUMENT (ATBD)

FOR THE THIRD ACTIVE CAVITY RADIOMETER IRRADIANCE MONITOR EXPERIMENT (ACRIM III)

ONE OF THE 24 OBSERVATIONAL COMPONENTS OF THE EARTH OBSERVATION SYSTEM (EOS)

PRIMARY SCIENCE OBJECTIVE: EXTENSION OF TOTAL SOLAR IRRADIANCE TIME SERIES AND ANALYSIS OF ITS VARIANCE FOR CLIMATOLOGICAL AND SOLAR PHYSICAL SIGNIFICANCE

ORIGINAL VERSION: 11/15/96, REVISED 12/15/99

PRINCIPAL INVESTIGATOR:

DR. RICHARD C. WILLSON
CENTER FOR CLIMATE SYSTEMS RESEARCH, COLUMBIA UNIVERSITY
1001 B AVE., #200, CORONADO, CA, 92118
PHONE: 818-585-9362 FAX: 818-585-9365
E-MAIL: acrim@acrim.com

CO-INVESTIGATORS:

DR. JAMES HANSEN
DIRECTOR, NASA GODDARD INSTITUTE FOR SPACE STUDIES
2880 BROADWAY, NEW YORK, NY, 10025
PHONE: 212-678-5500 E_MAIL: cmjeh@venus.giss.nasa.gov

DR. ALEXANDER MORDVINOV
INSTITUTE OF SOLAR-TERRESTRIAL PHYSICS,
RUSSIAN ACADEMY OF SCIENCES
P.O. BOX 4026
IRKUTSK, 664033, RUSSIA
E_Mail: avm@iszf.ru

DR. HUGH H. HUDSON
SOLAR PHYSICS RESEARCH CORPORATION
C/O Y. OGAWARA, ISAS, 3-1-1 YOSHINODAI
SAGAMIHARA, KANAGAWA, JAPAN
EMAIL: hudson@isass6.solar.isas.ac.jp

Table of Contents

1.0 Introduction

2.0 Overview and Background Information

- 2.1 Experiment Objectives
- 2.2 Historical Perspective
  - 2.2.1 Background
  - 2.2.2 Development of solar irradiance monitoring experiments
  - 2.2.3 Early space-based solar observations
  - 2.2.4 Sounding rocket experiments
  - 2.2.5 Nimbus7/ERB experiment
  - 2.2.6 SMM/ACRIM I experiment
  - 2.2.7 Solar monitoring by the ERBS experiment
  - 2.2.8 UARS/ACRIM II experiment
  - 2.2.9 Spacelab, ATLAS and EURECA experiments
  - 2.2.10 SOHO/VIRGO experiment
- 2.3 Instrument Characteristics

3.0 Algorithm theoretical discussion

- 3.1 TSI variability - observational evidence and physical interpretation
  - 3.1.1 Variability on solar cycle time scales
  - 3.1.2 Level of significance of the long term TSI
  - 3.1.3 Variability on solar active region time scales (days to months)
    - 3.1.3.1 The sunspot deficit effect
    - 3.1.3.2 Facular excess effect
    - 3.1.3.3 Energy balance in active regions
    - 3.1.3.4 Short term variability - solar global oscillations
- 3.2 Empirical models of TSI variability
  - 3.2 .1 Active region time scales
  - 3.2.2 Solar cycle time scales
  - 3.2.3 Shortcomings of linear regression models
  - 3.2.4 Multivariate spectral analysis

3.3 Constructing the long term Climate TSI database

3.3.1 Total solar irradiance monitoring strategy
3.3.2 Relating SMM/ACRIM I and UARS/ACRIM II results

3.4 EOS/ACRIM instrument description

3.4.1 Active Cavity Radiometer (ACR) sensors
3.4.2 Active Cavity Radiometer operation
3.4.3 EOS/ACRIM sensor technology considerations
3.4.4 Development of smaller ACRIM instruments - two approaches
3.4.5 Selection of the ACR VI instrument design for EOS/ACRIM

3.5 Theory of Active Cavity Radiometer measurements

3.5.1 Basic properties of the Active Cavity Radiometer
3.5.2 Derivation of the quasi-equilibrium equation
3.5.3 Discussion of the quasi-equilibrium equation
3.5.4 Form of the quasi-equilibrium equation terms

3.5.4.1 Cavity heating power term
3.5.4.2 Cavity heat capacity term
3.5.4.3 Radiation from the cavity to its surround
3.5.4.4 Radiation to the cavity from surround
3.5.4.5 Conductance to the heatsink from the cavity
3.5.4.6 Conductance to heatsink through leads

3.6 Uncertainty of ACRIM TSI measurements

3.6.1 General considerations
3.6.2 Root-mean-square uncertainty
3.6.3 Effects of temperature drifts

3.7 Data plan summary

3.7.1 Introduction
3.7.2 EOS/ACRIM data flow
3.7.2.1 ECS-ACRIM III SIPS functional interface
3.7.2.2 Network topology
3.7.3 ACRIM data types and volumes
3.7.3.1 Standing order descriptions
3.7.3.2 Baselined products according to SPSO database
3.7.3.3 ACRIM III SIPS for delivered to LaRC DAAC
3.7.3.4 Delivered algorithm package
3.7.3.5 Browse data

3.7.3.6 Other data and information transfers
3.7.3.7. Test data

3.8 Data processing specifications

3.8.1 Level 0 data
3.8.2 Level 1data
3.8.3 Level 2 data
3.7.4 Data volumes and rates

3.9 Data production schedule

4.0 Algorithm descriptions

4.1 Algorithm design heritage
4.2 Algorithm mathematical basis

4.2.1 Level 1A data - conversion to S.I. Units
4.2.2 Level 1B data - corrections for observational perturbations
4.2.3 Level 1C data - the time ordered series of in-situ TSI
4.2.4 Level 2 data - correction to 1 Astronomical Unit

4.2.4.1 Correction for the Earth - Sun distance
4.2.4.2 Correction for ACRIMSAT - Earth distance
4.2.4.3 Determination of ACRIMSAT - Sun distance
4.2.4.4 Relativistic effect of ACRIMSAT - Sun relative velocity

4.2.5 Level 3 data - TSI time series
4.2.6 Level 4 results - Correlations and time series analyses

4.2.6.1 Overview
4.2.6.2 Analysis of the primary data
4.2.6.3 Correlations
4.2.6.4 Time series analyses
4.2.6.5 Special analyses
4.2.6.6 Solar secular variation

4.3 Calibration

4.3.1 Metrology of the ACR measurements
4.3.2 Theoretical analysis of ACR calibration
4.3.3 In-flight calibrations
4.3.4 Comparison of multiple ACRIMSATs

4.4 Validation

4.1.1 Validation of Level 0 data
4.1.2 Validation of Level 1 data
4.1.3 Validation of Level 2 data

4.5 Quality control

5.0 Response to recommendations and comments from 1st review.

6.0 References

1.0 Introduction

This Algorithm Theoretical Basis Document (ATBD) is for the primary experimental objective of the EOS/ACRIM experiment whose basic scientific objectives and approach were defined in a proposal entitled "Active Cavity Radiometer Irradiance Monitor for the Earth Observation System program". This proposal was submitted to NASA Headquarters in July 1988 by Dr. Richard C. Willson, then with the Jet Propulsion Laboratory, in response to NASA Announcement of Opportunity OSSA-1-88. The ACRIM investigation was selected for the EOS program with Dr. Richard C. Willson as the Principal Investigator (PI) and Dr. Hugh S. Hudson as a Co-Investigator (Co-I). The Principal Investigator has since moved to Columbia University and will conduct the Scientific Investigation under the auspices of that institution. The approach is set forth in a proposal submitted to NASA by Columbia University titled: A Proposal for the continuing conduct of the scientific investigation of the EOS/ACRIM experiment' and in the Statement of Work executed between the EOS Project Office and Columbia University. The flight hardware aspects of the ACRIM experiment will continue to be the responsibility of the Jet Propulsion Laboratory, as per a NASA approved Memorandum of Understanding executed between Columbia University and the Jet Propulsion Laboratory.

The EOS/ACRIM experiment is a science and cost effective approach for providing the continuation of the precision total solar irradiance (TSI) database and conducting relevant climatological and solar physics scientific investigations during the EOS Mission. The observational objective of the (ACRIM) experiment is the production of a TSI database with state-of-the-art precision during the three five year segments of the EOS mission, as required by NASA AO OSSA-1-88.

2.0 Overview and Background Information

2.1 Experiment Objectives

Sustained changes in the total solar irradiance smaller than 0.25 % may have been the prime causal factor for significant climate change in the past on time scales of centuries. (Eddy 1976, Lean et. al., 1992, SIGC 1994) The long-range objective of TSI monitoring is to provide a precision database for comparison with the climate record that will be capable of resolving systematic variability of a tenth of one percent on time scales of a century. The continuation of the climate TSI database during solar cycle 23, establishment of its precise relationship to previous and successive components of the database, and analysis of TSI variability on all time scales with respect to the climatological and solar physics significance comprise the primary objective of the ACRIM experiment.

The science objectives of the EOS/ACRIM experiment fall into the two general categories of climatology and solar physics. The synergy between these disciplines was found to provide a productive research environment for the investigators analyzing data from similar previous solar monitoring experiments.

A primary objective of the experiment is observational: to monitor the variability of total solar irradiance, extending the NASA high precision solar total irradiance variability database into solar cycles 23 and 24. This database has been compiled as part of their earth radiation budget 'principal thrust' responsibility in the National Climate Program. ACRIM flight experiments have provided the precision database from the peak of solar cycle 21 (1980) to the present, except for a two year gap between the end of the SMM/ACRIM I (1989) and beginning of the UARS/ACRIM II (1991).

A second objective is the analysis of relationships between TSI and other variable aspects of the solar magnetic cycle. Significant new discoveries in both climatology and solar physics were derived from correlations between solar active region phenomena and the solar total flux variability monitored by the ACRIM I experiment. Analysis of such correlations would be made on time scales ranging from days to centuries using wavelet analysis of the TSI time series.

A third objective is the investigation of solar global oscillation phenomena. Helioseismology, the detection and analysis of solar oscillation modes, can provide physical information about solar processes deep within the sun that are inaccessible by other means. Solar global oscillations were detected in the ACRIM I total irradiance data, including pressure modes and possible gravity modes. A similar helioseismological analysis of the EOS/ACRIM TSI results will be conducted.

2.2 Historical Perspective

Detection of variability in the total solar irradiance, the energy supplied to the earth by the sun, has been a goal of mankind or more than a century. The stimulus has been the joint realizations that TSI is the primary determining factor of the earth's climate, and that the climate has varied significantly in the past. At any time in the earth's history the total solar irradiance, atmospheric chemical composition and the distribution of oceans and land masses have acted in combination to determine the earth's radiative balance, and hence the climate, of the biosphere.

In recent years the science of paleoclimatology has made great advances in understanding past climate changes and their causal mechanisms. On the time scale of billions of years, solar luminosity is thought to have increased about 30 % during the evolutionary cycle of the sun. About a billion years before present (BP) the increase in total solar irradiance combined with changes in the composition of the earth's atmosphere to provide a climate that could support life. The largest climate changes during the existence of life on earth were most likely of non-solar origin. Some were caused by volcanism: sea floor spreading that moved the continental landmasses and changed the topology of the ocean basins. The resulting alterations of ocean circulation - the primary heat exchange mechanism for the earth’s climate - resulted in major climate changes. Others may have been caused by the impact of extra-terrestrial objects such as asteroids or large meteorites. The most recent large-scale climate change began about 65 million years ago and continues into the present.

On 20 - 100 thousand year time scales periodic variations in the earth’s orbit, the so-called Milankovich effects have induced an effective variation of the total solar irradiance of the earth. The record of resulting climate variations has been detected in the deposition of the calcareous remains of benthic formanifera and the ratio of oxygen isotopes found in cores of sea floor sediment. (Hays et al. 1976) While this isn’t an example of intrinsic solar variability, it is a dramatic demonstration of the climatic impact of subtle solar irradiance variations.

The magnetic 'activity' cycle of the sun is known to have varied in periodicity and magnitude. Variations over the last several millennia are chronicled by the varying abundances of 'cosmogenic' isotopes, notably ^{14}C in living and fossil organic materials and ^{10}Be in Greenland ice cores, and by historical records of aurorae sightings. (Beer et al. 1991, Damon & Sonnet 1991) During the past several millennia, variations of climate and solar activity are correlated with periodicities near 11, 22, 88, 208 and 2300 years (See Table 2.2.1). While TSI variations were suspected as the cause of these changes, observations linking TSI and solar activity variations were not available until recently.

Table 2.2.1 Known climate variations related to solar variability.

CLIMATE PERIODICITY (YEARS)	RELATED TSI PERIODICITY	OBSERVED OR MODELED SOLAR PHENOMENA
11	Sunspot cycle	Solar active regions
22	Solar magnetic cycle	Active region polarity
88	Solar magnetic cycles	Aurorae
208	Solar activity minima	Cosmogenic isotopes
2300	Solar activity minima	Cosmogenic isotopes
20, 40 & 100 x 10^3	'Milankovich' cycles	Cosmogenic isotopes
10^9	Stellar evolution	Stellar model

2.2.1 Background

As science uncovered evidence that the earth's climate has varied in the past, the possibility that variations in total solar irradiance might be a cause of climate change stimulated research aimed at detecting solar variability. Experiments from ground based observatories, most notably those of the Smithsonian Astrophysical (1902-1962), and from aircraft, balloons, sounding rockets and satellites during the 1960's and 70's, were unable to detect total irradiance variations that were unambiguously solar in origin. (See Table 2.2.2.) These early efforts were frustrated by two principal limitations: uncertainties due to (1) instrument calibration and (2) atmospheric attenuation who's combined effects were larger than intrinsic solar variability over the time scales of the observations.

2.2.2 Development of solar irradiance monitoring experiments

A new generation of total irradiance measurement instrumentation was developed during the 1960's and 70's. (Hayley 1964; Plamondon & Kendall 1965; Willson 1967, 1971, 1973, 1979; Kendall (1968), Kendall & Berdahl 1970, Geist 1973; Brusa & Frohlich 1972) These new electrically self-calibrating cavity (ESCC) solar pyrheliometers had higher precision and accuracy than their predecessors and could be operated automatically in space flight environments.

The prototype ESSC pyrheliometer with many of the essential features in use today was developed by Charles Abbot of the Smithsonian Astrophysical Observatory (SAO) in the first decade of the 20th century. (Abbot, 1908) The instrumentation advances that have facilitated spaced-based solar monitoring observations with useful accuracy and precision today are the result of implementing these SAO instrumentation concepts with modern technology, plus the introduction of two operational features: the so-called 'active cavity' operational mode and the differential measurement approach. (Willson, 1973)

The 'active cavity' operational mode is one in which the same thermodynamic state is maintained for the cavity sensor in both the solar observation (shutter open) and reference (shutter closed) phases of a measurement. The differential measurement approach utilizes only the differences between solar observation and reference values, eliminating measurement dependence on the International Practical Temperature Scale.

The 'active cavity' operation is achieved by using an electronic servosystem to provide electrical heating power for the cavity detector during both shutter open and closed phases of measurement. The power is controlled at the amount required to sustain constant relative, internal instrument temperatures in the two measurement phases. The measurement then reduces to relating the cavity heating power in the shutter open and closed phases and several other key sensor parameters to the International System of units (SI). Operation does not depend on the International Practical Temperature Scale and the observational uncertainties are reduced to differences between small terms in the two measurement phases. The combination of these techniques greatly decreases the overall measurement uncertainty.

2.2.3 Early space-based solar observations

The availability of space-based observation platforms did not produce immediate success in detecting intrinsic solar TSI, as can be seen in Table 2.2.2 which includes two space-based total solar irradiance experiments. The first was the Nimbus 6 Earth Radiation Budget (ERB) experiment launched in 1975. (Hickey et al 1978) There were several reasons for its failure including the fact that its sensor was not an ESCC device but a less accurate flat plate sensor that relied on a pre-flight ground-based calibration. The most significant factor was the large, uncalibratable sensor degradation. Since the sensor was not a cavity device there was no amelioration of the effect of the deterioration of its solar absorbing surface on the measurement.

The second early experiment was the Thermal Control Flux Monitor (TCFM) flown on the Mariner 6 and 7 spacecraft’s to Mars in 1969. (Plamondon 1969) The TCFM represented a substantial contribution in being the first space flight utilization of an ESCC sensor (although this capability was utilized only at the end of its mission). Limited resolution in the digital data stream and sensor drift during its space flight to Mars appear to have prevented the detection of true solar variability.

2.2.4 Sounding rocket experiments

The first full implementation of ESCC solar pyrheliometry in a space flight environment occurred as part of a series of sounding rocket flights (1976 -

1986). In 1976 an Active Cavity Radiometer (ACR) on the maiden flight of NASA's solar irradiance sounding rocket program made the first such solar observations. (Willson & Hickey 1977) Both the ACR and other cavity pyrheliometers have since been flown in the series with full or partial ESCC implementation (See Table 2.2.3). The rocket program's principal purpose was to provide independent calibrations of satellite solar irradiance sensors over the 1976 to 1986 period. (Willson 1984) The series was terminated when a new NASA program to accomplish the same objective was initiated using the space shuttle.

Table 2.2.2. Early solar total irradiance (TSI) monitoring experiments. None were able to detect intrinsic solar variability due to instrument calibration or atmospheric transmittance uncertainties. The results shown (except for the Smithsonian) have been corrected to the World Radiometric Reference and are reconciled to the mean Earth-Sun distance.

YEAR	EXPERIMENTOR EXPERIMENTER	INSTRUMENT & SENSOR TYPE	CALIBRATION APPROACH**	BASIS	TSI RESULT (W/M2)
1902-62	Smithsonian	Water Flow	ESCC	Ground	1346
1962-68	Kondratyev	Yanishevsky (1)	RS	Balloon	1376
1967-68	Murcray	Eppley (1)	RS	Balloon	1373
1967	Drummond	Eppley (1)	RS	Aircraft	1387
1968	McNutt	GSFC Cone (2)	ESCC	Aircraft	1375
1968	Kendall	PACRAD (2)	ESCC	Aircraft	1373
1968	Willson	ACR II (2)	ESCC	Balloon	1370
1969	Plamondon	TCFM (2)	ESCC-P	Space-craft	1362
1969	Willson	ACRIII (2)	ESCC	Balloon	1368
1975	Hickey	Nimbus6/ERB (1)	RS	Space-craft	1389
1976	Willson	ACR IV (2)	ESCC	Rocket	1368

* Sensor Type: (1) - cavity, (2) - flat surface.

** Calibration Approach (in order of decreasing accuracy): ESCC - Electrically self-calibrating cavity ESCC-P - Partial implementation of electrically self-calibrated cavity RS - Relative Sensor no cavity no self-calibration relies on pre-flight calibration.

2.2.5 The Nimbus7/ERB experiment

The first long-term space flight solar monitoring experiment utilizing a cavity sensor capable of electrical self-calibration was the Earth Radiation Budget (ERB) experiment on the Nimbus 7 spacecraft. The valuable TSI database from this experiment, beginning in late 1978 and continuing to early 1993, is the longest currently available. (Hickey 1980, 1982, Hoyt 1990, Kyle et al. 1993) The Hickey-Freidan (HF) solar sensor was added to the ERB experiment to provide solar total irradiance insolation observations for the Earth Radiation Budget experiment with an accuracy better than +/- 0.5 %. This and more was certainly achieved, yet the full potential of ESCC sensors cannot be realized on this type of 'nadir-staring', polar orbiting platform without an independent solar pointing subsystem.

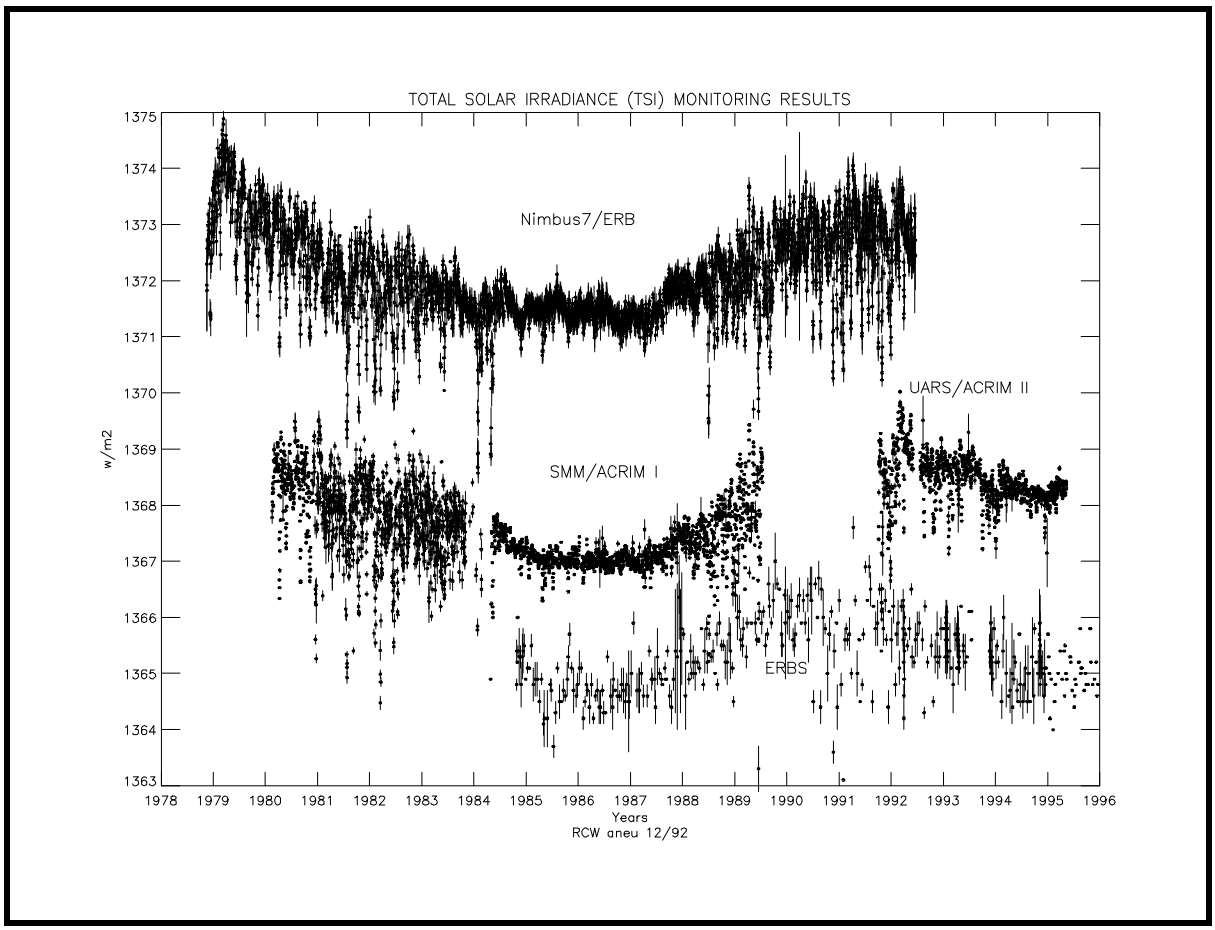

Figure 2.2.1.1 The record of TSI variability observations from spacecraft monitoring.

Table 2.2.3. Results from the NASA sounding rocket total solar irradiance rocket flight experiments

INVESTIGATOR	INSTRUMENT (NOTE 1)	1976 W/M2	1978 W/M2	1980 W/M2	1984 W/M2	1986 W/M2
Willson	ACR402 (1)	1368.1	1367.1	1367.8	1367.4	1367.1
Kendall	PACRAD (2)	1364	1373	1373		
Hickey	ESP (2)	1369	1387	1377		
Hickey	ERB (3)	1389	1387	1377		
Hickey	HF (2)			1376		
Frohlich	PMOD (1)				1366.7	1366.8

Note 1: Instruments: ACR = Active Cavity Radiometer, PACRAD = Passive Absolute Cavity Radiometer and Detector, ESP = Eclectic Solar Pyrheliometer, ERB = engineering model of Nimbus6 Earth Radiation Budget solar sensor, HF = Hickey - Freidan radiometer, PMOD = Physical Meteorological Observatory of Davos (Switzerland) radiometer. Sensor operational modes: (1) ESCC, (2) ESCC-P, RS.

The absence of an independent solar pointing for the ERB was one of its principal sources of uncertainty. It severely limited solar observation time to a few minutes per orbit near the terminator while the sun swept through its field-of-view. Additional measurement uncertainty accrued due to off-axis irradiation of the cavity that perturbs its thermal balance and causes departures from theoretical performance. Measurement uncertainty also derived from temperature dependent calibration errors - the result of infrequent operation in the ESCC mode (once every two weeks).

The combination of the above factors sustained a noise level in the Nimbus 7/ERB TSI database that inhibited recognition of intrinsic solar variability features until detected by another solar monitoring experiment in 1980 (see next section). Once discovered, however, clear evidence of solar variability on active region and solar cycle time scales were found in the ERB results. The corroborative function of the ERB data has been of great significance in verifying solar variability on solar cycle time scales. These results are available from the National Space Science Data Center Archives. The Nimbus 7/ERB results are shown in Figure 2.2.1.1.

2.2.6 The SMM/ACRIM I experiment

The Active Cavity Radiometer Irradiance Monitor (ACRIM I) experiment launched on the Solar Maximum Mission (SMM) in early 1980 was specifically designed to provide the start of a long term, high precision solar total irradiance climate database. (Willson et al. 1981) The first in a series of satellite

experiments in the NASA solar monitoring program, the ACRIM I experiment produced a high precision database throughout the 9.75 years of the Solar Maximum Mission. This included a period between late 1980 and early 1984 affected by solar pointing limitations during which time the number of daily observations decreased and their uncertainty increased. Observations ceased in October 1989 when the SMM satellite re-entered the earth's atmosphere. The results of the ACRIM I experiment are included in Figure 2.2.1.1. These results are available from the National Space Science Data Center Archives.

The smaller measurement uncertainty of the ACRIM I results, relative to those of the Nimbus7/ERB, are attributable to its continuous 'active cavity' ESCC mode of operation, its degradation self-calibration capability and the SMM's full time solar pointing. Its shutters opened or closed every 65 seconds, providing electrical self-calibration before and after each solar observation. It employed three independent ACR sensors with different duty cycles to provide internal calibration of cavity optical degradation (See figure 2.2.2). Precision references calibrated its electrical measurement system continuously. The solar pointing of the SMM provided acquisition of large numbers of daily observations (10^4 during normal operations, 10^2 during the 1981-84 'spin mode' of solar pointing), providing small statistical uncertainties of average daily values.

The ACRIM I results of early 1980 provided the first unequivocal evidence of intrinsic solar variability. (Willson 1980) Solar variations have since been detected on every observable time scale, from the experiment's 1.024-second sampling interval, to the duration of the Mission. (Willson et al 1981; Willson 1982, 1984; Hudson et al. 1982; Hudson & Willson 1982; Willson & Hudson 1981, 1988, 1991)

2.2.7 The ERBS experiment

A new generation Earth Radiation Budget experiment (ERBE) was launched as the NASA Earth Radiation Budget Satellite (ERBS) in 1984. (Barkstrom et al. 1990, Lee et al. 1995) Most of the operational constraints of the Nimbus7/ERB experiment affect the ERBS TSI measurements as well. While they use sensors nearly identical to those on the ACRIM I experiment, and in a fully implemented ESCC mode during solar observations, the quality of data is fundamentally limited by minimal solar viewing opportunities, on the order of minutes during a single orbit during one day every second week as the sun sweeps through their (large) field of view. They acquire observations that meet the requirements of the earth radiation budget modeling objectives but have marginal precision, observational frequency and persistence for the climate TSI monitoring database. As can be seen in figure 2.2.3, the ERBS results show much larger scatter and uncertainty than those of the ERB, ACRIM I and ACRIM II, a direct consequence of the paucity of observations and the constraints imposed by the 'nadir-staring' platforms on which it resides without independent solar pointing.

2.2.8 The ACRIM II experiment on the Upper Atmosphere Research Satellite

The ACRIM II experiment was launched in September 1991, nearly two years after the end of the Solar Maximum Mission. The results are shown as figure 2.2.4. The launch was delayed several years by the Challenger accident and prevented the planned direct on-orbit comparisons between ACRIM I and II. The importance of relating their results through in-flight comparisons cannot be overstated. The absolute uncertainty of flight TSI sensors is about 0.1 % in the laboratory and up to several times larger in space flight experiments - inadequate to sustain a useful long term TSI database. Evidence for this is clearly seen in Fig. 2.2.1.1: the spread of results from the ERB, ACRIM I & II and ERBS experiments covers about +/- 0.3 % about their mean, which is three times the solar cycle 21 peak-to-peak TSI variation. Fortunately for the TSI database, the two ACRIM experiments were overlapped by the Nimbus7/ERB and ERBS observations and it has been possible to relate ACRIM I and II with these comparisons as described in section 3.3.

2.2.9 Spacelab 1/ACRIM, ATLAS/ACRIM and EURECA TSI Experiments

Several shorter-term TSI experiments have been conducted in space flight experiments. The first were the ACRIM and CROM experiments on the Spacelab 1 Mission in 1983. Sequels to these experiments were conducted on the space shuttle in the ATLAS 1, 2 and 3 Missions in 1992, 1993 and 1994. Two ESA TSI experiments, the PMOD (Brusa & Frohlich 1972) and CROM (Crommelynck 1981) were on the European Recoverable (EURECA) platform, which was launched by the shuttle in 1992 and retrieved in 1993.

The principal purpose of the shuttle based ACRIM and CROM experiments flown on the Spacelab and ATLAS Missions was to make comparisons with satellite TSI monitoring experiments as part of the ‘overlap strategy’. The results are shown in Table 2.2.4.

The Spacelab 1/ACRIM data was acquired during the SMM/ACRIM I mission. The ATLAS/ACRIM results were acquired during the UARS/ACRIM II experiment. In the interest of understanding the reliability of the shuttle ACRIM results, the ACRIM II observations are scaled to ACRIM I as discussed in section 3.3.2, to facilitate comparison of Spacelab 1 and ATLAS measurements. Sensor ACR502 was included in the ACRIM instrument on all three shuttle flights, the ACR504 on two. The weighted means are dominated by the ATLAS results because of their smaller uncertainties. This is caused by the far smaller number of observations acquired during the Spacelab 1 Mission when near total failure of the shuttle command-and-data system (RAU) occurred.

The spread of the observations from the flights (+/- 242 ppm for ACR502 and +/- 152 ppm for ACR504) exceeds their statistical uncertainties by a large margin, indicating the clear intervention of sources of systematic error. It has been observed that the cavities of the ACRIM sensors are contaminated when turned for re-calibration after each flight, which is believed to be the principal cause of the variation of results from flight-to-flight. The largest spread is between the ACR502 result of ATLAS1 and the other two, indicating that its 2nd flight result could be anomalously high. This may be resolved by the ATLAS3/ACRIM experiment.

It was hoped that the shuttle ACRIM series would be able to provide mission-to-mission precision better than 100 ppm instead of the approximately 200 ppm observed from the results to date. While larger than expected, it is an order of magnitude superior to the absolute uncertainty of the current generation of sensors that operate at ambient temperature, and comparable to the absolute uncertainty of cryogenic TSI sensors currently under development.

The ESA URECA platform was launched from the shuttle in mid 1992 and retrieved bout nine months later. Two TSI monitors resided on the platform: the PMOD developed by Frohlich and the CROM developed by Crommelynck. (Frohlich 1993, Crommelynck 1993) Comparisons of preliminary daily mean results obtained simultaneously by the EURECA/PMOD and the UARS/ACRIM II experiments demonstrated that they depict essentially the same principal TSI variations, including the 'sunspot deficit' effects of large sunspot groups in the early and late part of the period.

2.2.10 The SOHO/VIRGO experiment

The Solar and Heliospheric Observer (SOHO) spacecraft was launched in December 1995 toward its parking orbit at the L1 Lagrangian point between the earth and the sun. One of the experimental packages on board SOHO is the Variability of solar Irradiance and Gravity Oscillations (VIRGO) experiment. VIRGO measures the TSI with active cavity radiometers (PM06-V and the Dual IRradiance Absolute Radiometer, DIARAD), the spectral irradiance by a three channel Sunphotometer (SPM) and the radiance for global oscillation studies with a 12-resolution element Luminosity Oscillations Imager (LOI).

Preliminary results and findings have been reported as successful, although the primary TSI instrument on-board, the PM06-V, operates in a degraded mode without a functional shuttering system. Several gaps in the VIRGO TSI database have occurred due to problems with the SOHO spacecraft. The relationship of pre and post gap TSI results from VIRGO has been deduced through comparisons with the UARS/ACRIM II experiment –a further testament to the importance of redundancy in TSI monitoring. Significant degradation in the form

of altered sensor behavior was detected after a lengthy (~ 6 month) gap in 1998 during which instrument temperatures became extremely cold.

Table 2.2.4 Results from the space shuttle ACRIM experiment on the Spacelab 1, ATLAS 1 & 2 Missions.

MISSION	DATE	SENSOR	UNCER-TAINTY	SENSOR	UNCER-TAINTY
		ACR502	Std.Err. (σ)	ACR504	Std.Err. (σ)
		(% Var.)	(% Var.)	(% Var.)	(% Var.)
Spacelab 1	12/93	0.3679	0.0098	0.4479	0.0088
ATLAS 1	3/92	0.4164	0.0028	Na	Na
ATLAS 2	4/93	0.3680	0.0006	0.4174	0.0007
Weighted Mean (All Flights)		0.3701	0.0006	0.4176	0.0007
Weighted Mean (ATLAS Flights)		0.3701	0.0006		
Weighted Mean (SL1 & ATLAS 1)		0.3680	0.0010	0.4176	0.0011

2.3 Instrument Characteristics

Table 2.3.1 below summarizes the instrumentation and observational requirements for the EOS/ACRIM experiment. The sensor technology selected for the first ACRIM instrument is the ACR type IV. The size of the round primary apertures is to remain the same as previous ACRIM instrumentation: 0.5 cm^2. Apertures should be made of aluminum, as precisely round as possible, with knife-edges and polished surfaces. Aperture area must be measured with the maximum possible state of the art accuracy, traceable to NIST.

The field of view is to be the same as for the SMM/ACRIM I and UARS/ACRIM II sensors: 2.5 deg. half angle defined from the center of the primary aperture along the center of the viewing axis through the view limiting aperture. The 'shading angle' is defined as the maximum tolerance for off-sun pointing and is defined as the angle of off-sun pointing that causes the geometrical shadow of the view limiting aperture's edge to fall on the edge of the primary aperture. This angle is to be 1.0 degree. The tolerance in flight for solar pointing is to be 0.5 degree, to prevent approaching near enough to the shading angle to require significant correction for diffraction.

The ACR IV cavities will be mounted in individual sensor modules like those employed in the UARS/ACRIM II instrumentation. These modules provide the thermal mass and isolation necessary to minimize their susceptibility to thermal drift of the external parts of the instrument. The modules will, in turn, be isolated from the external thermal environment. The temperature rate of change of the ACR IV sensors' copper mounting flanges must be kept below 0.01 K per shutter cycle during solar observations.

The view limiter baffling is to be accomplished using a single baffle as in the UARS/ACRIM II design. The baffle's function is to prevent the sensor from viewing the walls of the view limiting assembly above the baffle and prevent extreme rays entering the view-limiting aperture from falling on the walls below the baffle.

Each sensor is to have an independently operable shutter. The side of the shutters facing the sun are to have UV-stable, high solar reflectance, high IR emmitance surfaces to minimize solar heating. The side of the shutters facing the primary apertures is to have high IR reflectance and low IR emmitance surfaces to minimize the contribution of IR emmitance to the measurement.

The shutter cycle will continue to be symmetrical, as in previous ACRIM's, with a shutter operation every 65.536 seconds. The shutters of all cavities must be commandable via uplink to provide all possible combinations of cavities for solar observations in both automatic and manual modes.

The servosystem for the sensors must produce final measurement values of cavity heater current and voltage settled to within the A/D conversion least significant bit of final value within less than 30 seconds of shutter operation. Resolution of the A/D converter will be 16 bits or greater. The sensor must be able to respond to a TSI range of approximately 2000 W/M^2 to accommodate the irradiance near perihelion.

The nomenclature for the instrument is to be the Active Cavity Radiometer type VI (ACR VI). Each flight instrument launched in the EOS/ACRIM program will be referred to as a numbered ACRIM beginning with III.

The preferred orbit is geosynchronous because it provides nearly 99 % annual solar exposure. Second preference is for high inclination polar 'near earth' orbits (~ 90 degrees) to provide maximum solar exposure. Polar orbits must have nominal altitudes greater than 600 KM to provide five year mission lifetimes in the absence of additional boosting, and less than 1000 KM to avoid excessive radiation environments. In all orbits, annual average solar observation time per orbit must be > 55 minutes.

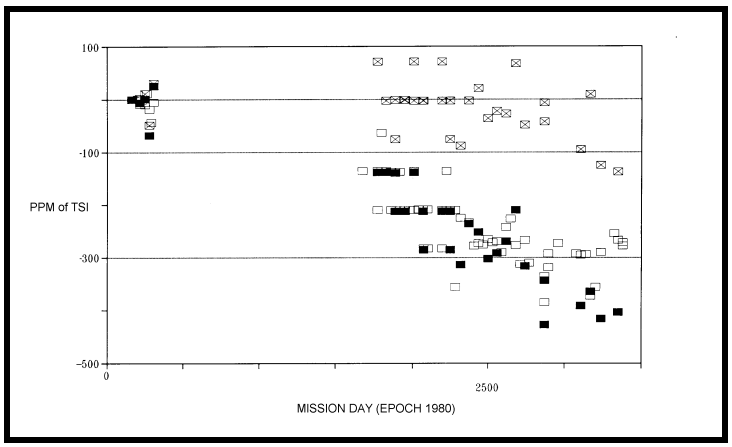

Figure 2.2.2 Degradation calibrations of the Solar Maximum Mission ACRIM I experiment. Solid black squares are the ratios of ACRIM I sensors A (the continuously monitoring cavity) and C (the least frequently used calibration cavity). Open squares are the ratio of A and B (the most frequently used calibration cavity). Crosshatched squares are the ratio of sensors B and C.

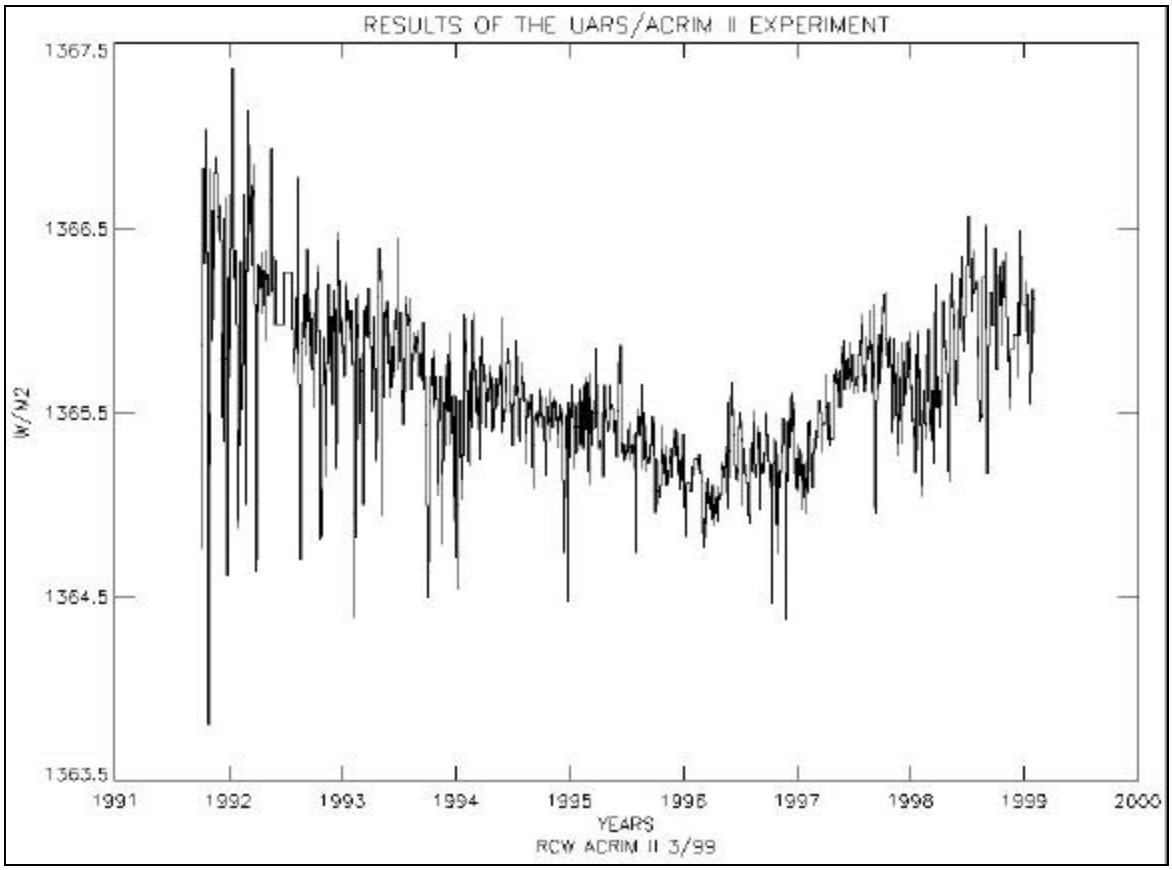

Figure 2.2.3 Total Solar Irradiance observations of the ACRIM II experiment on the Upper Atmospheric Research Satellite. Daily mean results.

Table 2.3.1 EOS/ACRIM INSTRUMENT PARAMETERS AND REQUIREMENTS

Quantity	Description
Sensors	Three Type IV Active Cavity Radiometers Equivalent to SMM/ACRIM I sensors
Primary Apertures	0.5 cm. 2, round, Aluminum Maximum accessible area accuracy, traceable to NIST Knife edge and polished aluminum surfaces
Cavity geometry	30 degree Right circular cone Minimize paint meniscus at apex
Sensor configuration	Cavities mounted in individual modules Equivalent to UARS/ACRIM II modules
Cavity Absorber	Specular black epoxy paint
Field of View	+/- 2.5 degree, conical from center of primary aperture Centered on instrument line of sight View limiting aperture → +/- 0.5 degree shading angle
Solar Pointing	Instrument line of sight maintained within 0.5 degree of sun's center
Heatsink	Passive sensor module equivalent to UARS/ACRIM II
Baffling	Single baffle, shades primary aperture from upper view limiter walls. Shades lover view limiter walls from extreme rays through view limiting aperture.
Shutter surfaces	Solar side: high solar reflectance, high IR emittance Sensor side: low IR emittance, high IR reflectance
Sensor settling time	< 30 seconds to +/1 LSB of A/D conversion
Accuracy	99.8 % at TSI level
Precision	A/D resolution: 16 bit Single sample: +/- 0.003 % of full scale TSI
Ranges	Total irradiance: ~ 0 - 2000 W/m2 Wavelength: ~ 0.001 - 12000 um
Shutter Operation	Open or close every 65.536 seconds on active shutters All combinations of sensors accessible in automatic and manual modes, via uplink command
Size/Mass/Power	Cylindrical: ~ 15 cm. diam. x ~ 30 cm long/~12 kg./TBD
Sensor Temperature Drift	< 0.01 K per shutter cycle at cavity copper button
Nomenclature	Sensor assembly: Active Cavity Radiometer VI (ACR VI) Experiment: EOS/ACRIM III & etc. as launched
Observation Time	> 55 min. on-sun per orbit (annual average)
Orbit	Geostationary preferred. If polar must be high inclination to meet observation time requirements and nominally > 600 km and < 1000 km altitude.

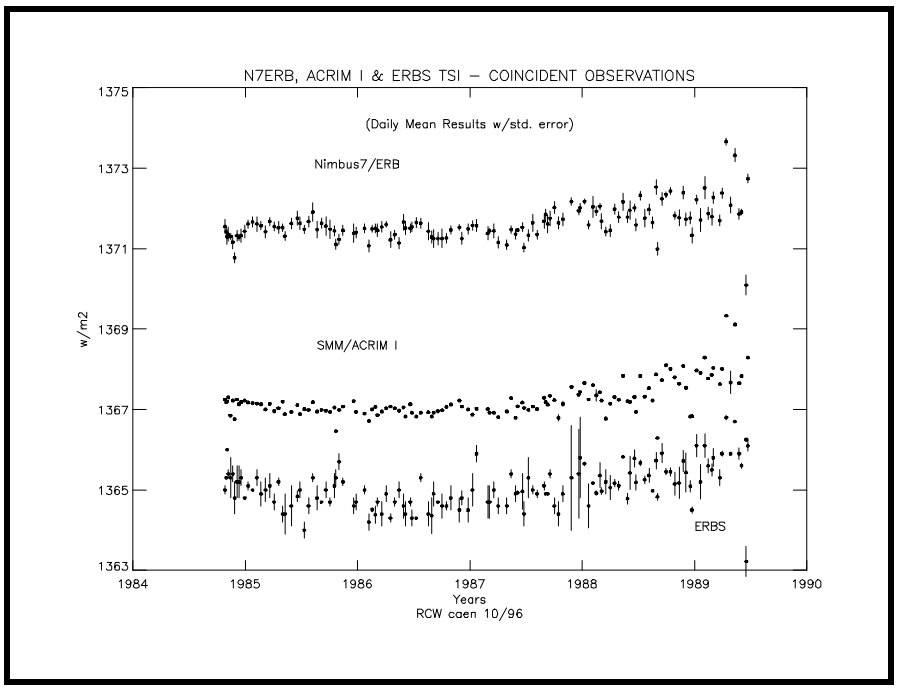

Figure 2.2.3.a Total Solar Irradiance observations of the Nimbus7/ERB, ACRIM I and ERBS experiments for days when all three had observations. Standard error of daily mean results shown as vertical tics.

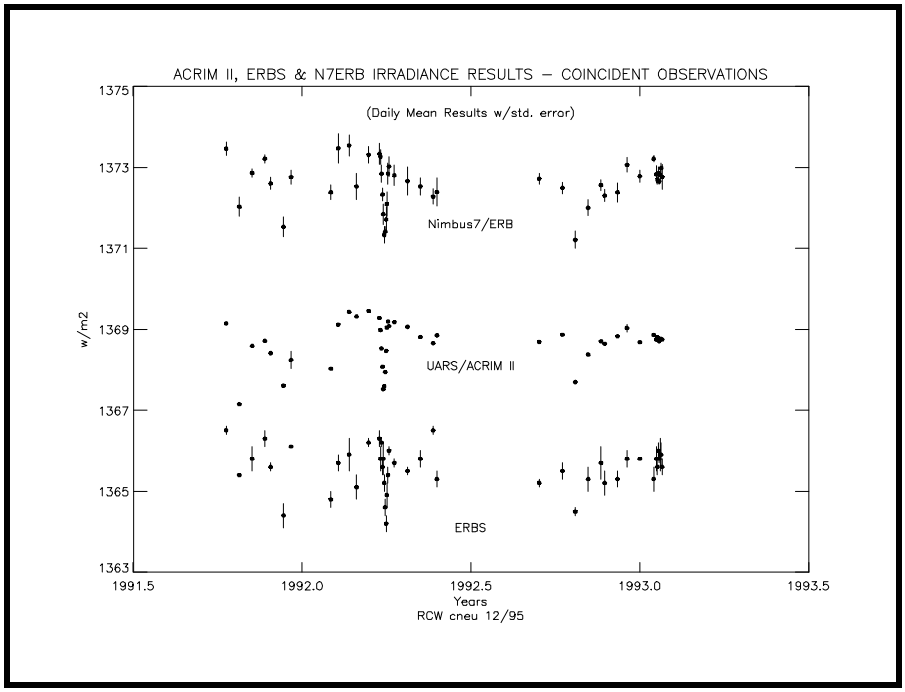

Figure 2.2.3.b Total Solar Irradiance observations of the Nimbus7/ERB, ACRIM II and ERBS experiments for days when all three had observations. Standard error of daily mean results shown as vertical tics.

3.0 Algorithm Theoretical Discussion

3.1 TSI variability - observational evidence and physical interpretation

3.1.1 Variability on solar cycle time scales

The results of monitoring total solar irradiance during solar cycles 21, 22 and 23 have proved significant to both solar physics and climate research. The high precision TSI database extends from late 1978 to 1999, longer than one solar (sunspot) cycle (~ 11 yr.), and nearly a solar magnetic cycle (~ 22 yr.).

The ACRIM I, ACRIM II, ERB and ERBS results shown in detail in figure 2.2.1.1 are based on the mean value daily observation database, normalized to the mean earth-sun distance. It can be seen that the gross features of the results, the decline from solar cycle 21 maximum to solar minimum and the increase to solar maximum of cycle 22 and the decrease toward the next solar minimum are basically the same for the observations from these experiments. There are some significant differences, however, most of which are assumed to be the effects of solar pointing and thermal errors and uncorrected sensor degradation in the ERB and ERBS results.

The difference in the precision of the observations is readily apparent from Fig. 2.2.1.1. It is especially noticeable during the minimum around 1986 when the solar noise component driven by solar activity subsided. The measurement uncertainty tics are barely visible for the ACRIM I experiment, clearly apparent for ERB and quite large for ERBS. During the ‘spin mode’ of solar pointing for the ACRIM I experiment (1981 - 1984) the measurement uncertainties were about the same as the Nimbus7/ERB. This was due to the wobbly spin mode that caused observations by ACRIM I to be made in a similar manner to those of ERB.

The apparent abrupt change in the level of fluctuation of ACRIM I results following the gap in early 1984 is an artifact of the transition from spin mode to precision pointed mode following repair of the SMM satellite's pointing system by the space shuttle, and the decreasing levels of solar activity during the period. The gap resulted from a paucity of data samples, caused by satellite data acquisition restrictions during the four months prior to the SMM shuttle repair mission. Had the SMM pointing system not failed, and the gap not occurred, a more gradual transition in variability of the database from the peak solar activity levels of1980-81 to the 1986 activity minimum would likely have been recorded. In support of this, a relatively gradual transition can be seen in the uninterrupted ERB results during 1984.

The average irradiance declined systematically from launch through mid 1986 at an average rate of 0.015 % per year. The irradiance minimum in 1986 occurs near the cycle magnetic minimum in September. The rapid increase, corresponding to the build- up of solar activity in cycle 22 becomes clearly visible in 1988, continuing to the end of the SMM/ACRIM I results in mid 1989, and on through the peak of solar cycle 22 as can be seen in the continuing results from the ERB, ERBS and UARS/ACRIM II experiments.

A significant divergence occurs after 1988 where the rate of irradiance increase in ACRIM I results exceeds that of ERB and ERBS. This was probably caused by uncalibrated degradation in the ERB and ERBS measurements as the level of high-energy solar particles and flux increased during the ascending phase of solar cycle 22. This was the same period in which significant degradation was observed to occur in ACRIM I's comparison sensor B.

The direct correlation of luminosity and solar activity is a major discovery from the solar cycle results. It agrees in sense with that predicted from the coincidence of the "Little Ice Age" climate anomaly and the "Maunder Minimum" of solar activity during the 16^{th} and 17^{th} centuries. (Eddy 1976) The average temperature decreased by between 0.5 and 1.5 Kelvin (k) in response to what models indicate was a total irradiance decrease of between 0.25 and 1.0 %. The A climate change in response to the 0.1 % peak-to-peak amplitude of the total irradiance during solar cycle 21probably be undetectable in the noise of seasonal and weather processes during a single solar cycle.

Another major discovery from these results is the apparent asymmetry of the solar cycle TSI variation relative to solar minimum. There is a gradual decrease from the maximum levels of solar cycle 21 to the minimum in 1986, followed by the rapid increase to the solar maximum of cycle 22. This again is followed by a more gradual decrease toward the minimum of solar cycle 22 in 1996-97. This is consistent with the shape of other monitored solar activity indices such as the Zurich sunspot number and the 10.7 cm. radio flux.

One of the most important climate findings from the long term TSI database is an apparent trend between the minima of the two successive solar cycles covered thus far. The results of successive Active Cavity Radiometer Irradiance Monitor (ACRIM) experiments have been related with sufficient precision using the Nimbus7/ERB results to resolve a multi-decadal, upward trend in total solar irradiance of 0.032 percent per decade between the minima of solar cycles 21 and 22. The trend follows the rising solar activity levels of recent decades and, if sustained, would add solar forcing to the 'greenhouse gas' forcing that is raising global temperatures and altering the climate. Systematic variation of total solar irradiance near the rate found has been implicated as a causal factor in climate change on century to millennial time scales. The trend is depicted graphically in figure 3.1.1.1. (Willson 1997) The ERBS results demonstrate a similar trend of

0.027 %/decade. While these two results appear to lie outside their bounds of mutual uncertainty for random errors, they agree quite well within the bounds of likely systematic errors. The agreement leaves little doubt that an upward trend occurred.

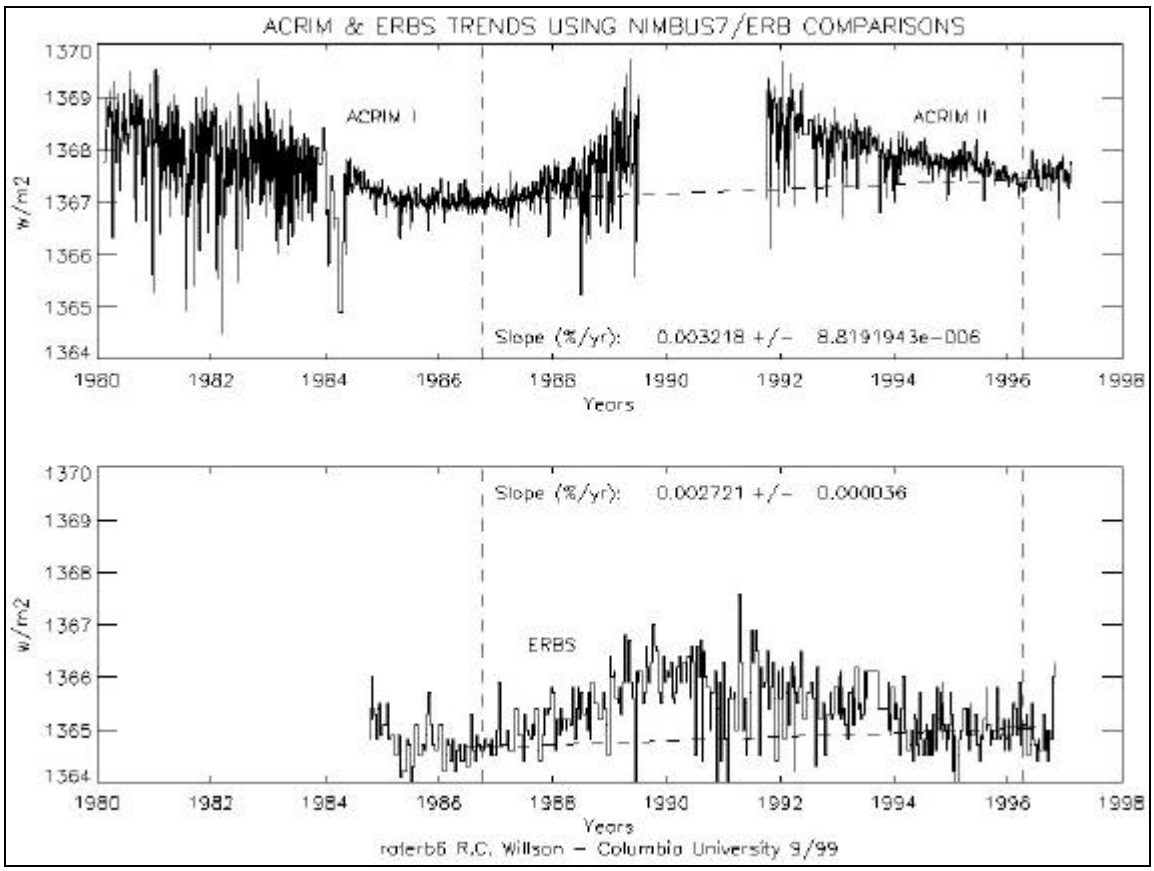

Figure 3.1.1.1 TSI trend between successive solar minima found in the composite ACRIM and the ERBS databases. The two results are outside their mutual sources of random error but agreement is likely well within the bounds of systematic errors.

3.1.2 Level of significance of the long term TSI database

Current state of the art TSI cavity sensors, operating at 'ambient' temperature (~20 ^{o}C) are able to define the radiation scale with about 0.1 % uncertainty in laboratory conditions and several times larger uncertainty in space flight experiments. This is inadequate to connect the results of successive TSI experiments and sustain the long-term climate TSI database. The peak-to-peak solar cycle TSI signal during solar cycle 21 was just 0.1 %. The spread of results over +/- 0.3 % of the mean in figure 2.2.1.1 is indicative of the absolute uncertainty of these devices in flight environments.

The long term precision of the ACRIM I, ERB, ERBS and ACRIM II databases is critically important to understanding the significance of their solar cycle results. The principal source of systematic error for ESCC sensors during flight is degradation of sensitivity of their solar absorbing surfaces caused by exposure to solar flux. Of these experiments, only the ACRIM's are capable of calibrating the degradation of their sensors. Over the 9.75 year mission ACRIM I's total degradation was about 600 parts per million (ppm) of the total irradiance. (See figure 2.2.2) After correction for degradation, the residual uncertainty was estimated to be 30 ppm. ACRIM II has experienced more degradation than ACRIM I but with the improvements in flight instrumentation and degradation calibration procedures, has residual uncertainties of below 20 ppm over the first five years of the UARS mission.

The period of missing data points in fig. 2.2.2 corresponds to the SMM spin mode when the average uncertainty of observations was larger than the total degradation during the period. Eventual degradation of sensor B is seen after about day 2500 (epoch 1980), as its solar exposure time accumulated and the level of high energy, degradation-inducing solar fluxes produced by the rising solar activity phase of cycle 22 increased. The linearity of the A/C ratio and the complementarity of the A/B and B/C ratios during the last 1000+ mission days combine to indicate that: (1) there was no significant sensor C degradation, (2) the B/C ratio continued to be predictably related to the prior observations, and (3) our assumption that the degradation of all sensors was proportional to exposure time and the level of solar activity was confirmed.

The solar observing times for each orbit of the ERB and ERBS experiments is about 5 - 10 minutes. The observing times for ACRIM I and II are 55 and 35 minutes/orbit, respectively. Since degradation is proportional to solar exposure, the rate of degradation of the ERB and ERBS sensors might be expected to be proportionately less than the ACRIM's. The relative rates of degradation cannot be computed precisely based on exposure time, however, since the cavity designs are sufficiently different that their degradation sensitivities to exposure will not be the same. The 'inverted cone' cavity design of the ERB places more of its absorbing surfaces closer to the instrument's aperture than in the ACRIM design, which would increase its rate of degradation by solar exposure. The ERBS sensors' relatively large fields of view, 15 deg. compared to ACRIM's 5 deg., also increase their degradation sensitivity.

No corrections have been applied for degradation of the ERB sensor to the results shown in figure 2.2.1.1. The generally good agreement between its results and those of ACRIM I is probably an indication that significant degradation did not occur during the first decade of its mission. A significant divergence of ACRIM I and the ERB and ERBS results can be seen in fig. 2.2.1.1 following solar minimum in which the ACRIM I's results increase more

rapidly. This probably indicates the accrual of significant degradation by the ERB and ERBS sensors during the rising activity portion of solar cycle 22. If this is the case, the relationship between ACRIM's I and II determined through comparisons with ERB and ERBS, and the quality if the long term climate TSI database will be adversely affected.

3.1.3 Variability on solar active region time scales (days - months)

3.1.3.1 The sunspot 'deficit' effect

An inverse relationship between sunspot area and solar total irradiance was discovered using ACRIM I results early in the SMM. (Willson 1980, 1984; Willson et al. 1981, Hudson et al. 1982; Hudson and Willson 1982; Chapman 1983; Chapman & Herzog 1986; Schatten et al. 1985) The major sunspot features can be seen in the Nimbus 7/ERB results as well. (Hickey et al. 1980; Hoyt 1990) As active regions containing sunspot area rotate onto, and/or form and grow on the earth side of the sun, a corresponding decrease in total irradiance is detected. These decreases last the duration of the transit of the sunspots and have been observed with amplitudes of up to - 0.25 % of the total irradiance. The so-called 'sunspot deficit' can be clearly seen in figure 3.1.1, a plot of the results from observations of ACRIM I in early in 1980 together with a solar spectroheliogram for the same period of time. This pattern was repeated many times, with varying detail, throughout 1980 as shown in figure 3.1.2.

A direct relationship between active region faculae and total irradiance was found in the ACRIM I results. (Willson et al. 1981, Willson 1984) Irradiance peaks were found to occur during the transit of active regions known to contain large facular areas. On other occasions the presence of large active region faculae were observed to partially offset the net irradiance deficit produced by sunspots, relative to deficits produced by comparable sunspot area when less faculae were present. The facular effects can be clearly seen in Fig.'s 3.1.1 and 3.1.2 as 'wings' on either side of the prominent sunspot 'deficits. Active region faculae have generally larger areas than sunspots and are more widely distributed around the periphery of active regions. This results in their being the first radiative component of an active region to be seen (from the Earth) as it rotates onto our side of the sun, and the last to be seen as it rotates off the opposite limb. The other effect, reduction in the sunspot 'deficit' is always present but more subtle. It can be seen in mid July 1980 (Fig. 3.1.2) where the relatively shallow 'deficit' corresponds to the 'deficit' effect of large sunspot area being partially offset by very large facular area.

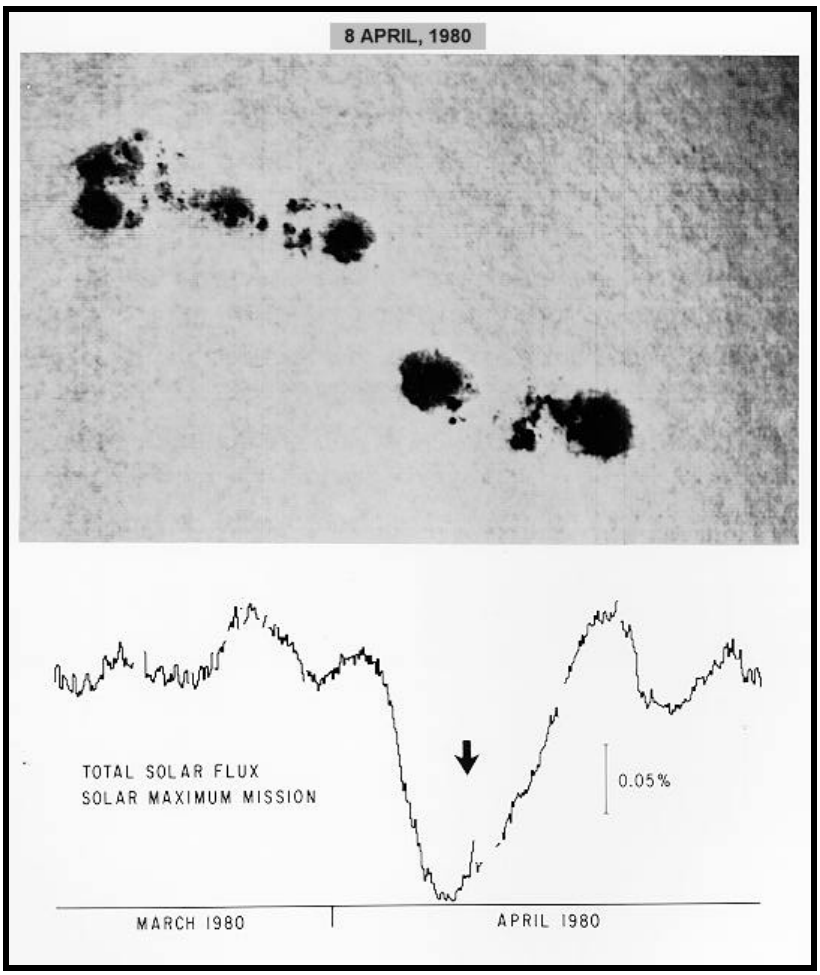

Figure 3.1.1 TSI variability showing the ‘sunspot deficit’ caused by two large spot groups in March and April 1980 detected by the SMM/ACRIM I experiment. The arrow indicates the location in the TSI time series of the sunspot spectroheliograph. The scale of TSI variability is set by the 0.05 % bar.

3.1.3.2 Facular 'excess' flux

3.1.3.3 Energy balance in active regions

The evolution and energy balance in active regions has been investigated using solar active region area measurements and the ACRIM I results. No two active regions evolve in the same way, but a general pattern was observed during sunspot maximum in solar cycle 21. Sunspot area, with its high contrast relative to the undisturbed photosphere (- 0.5), peaked quickly and subsided within several solar rotations (about 81 days). Faculae have less contrast relative to the 'quiet photosphere' (~ + 0.03) and slower development, but have larger areas and longer persistence than sunspots (up to 6 solar rotations). Indications are that the initial sunspot 'deficit' is substantially compensated over the 'lifetime'

of an individual active region by facular emission and the balance is dissipated into the extended solar atmosphere in the form of the 'active network'.

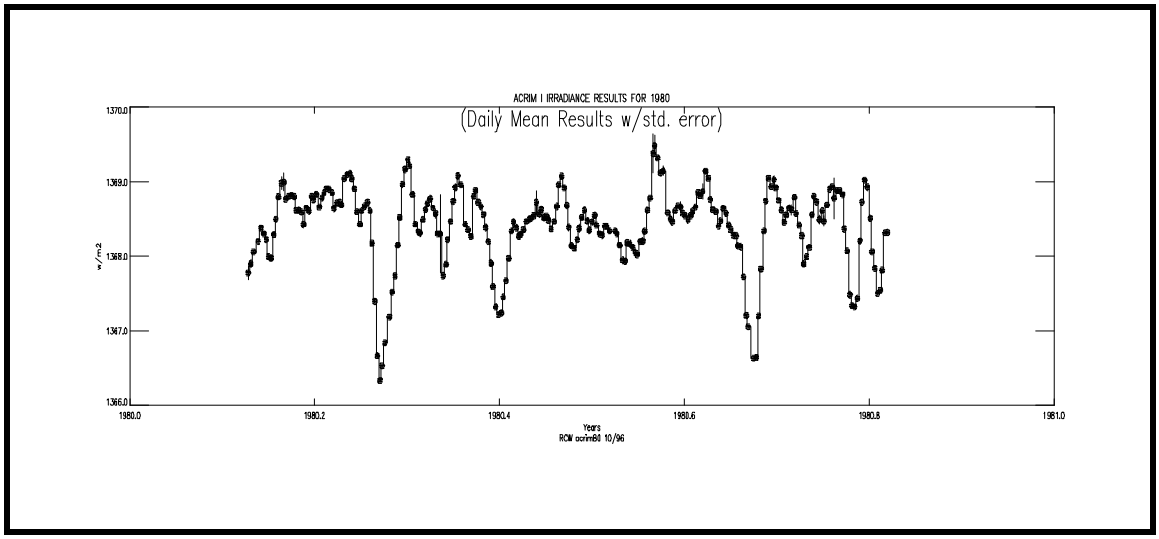

Figure 3.1.2 TSI variability observed by the SMM/ACRIM I experiment in 1980. Numerous occurrences of both ‘sunspot deficit’ and ‘facular excess flux’ are seen as decreases below the mean flux level and increases near the deficits.

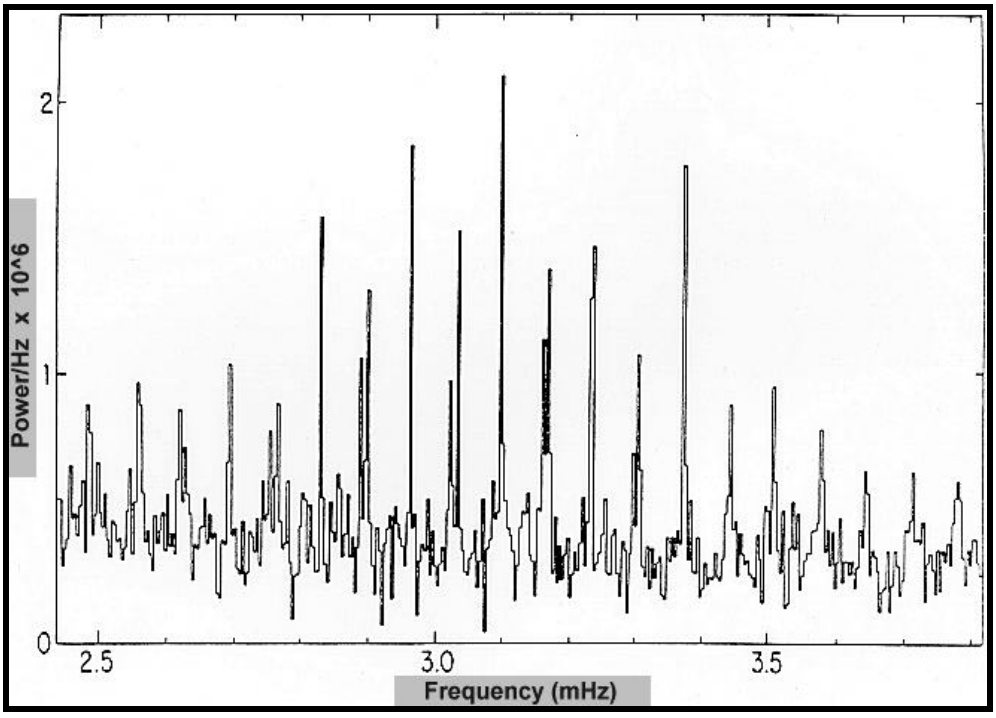

Figure 3.1.3 Pressure mode oscillations derived from ACRIM I shutter cycle database. Ordinate is power/Hz in units of parts per million of the TSI.

3.1.3.4 Short-term variability - solar global oscillations (minutes to days)

Solar global oscillations of low degree have been detected in the ACRIM I total irradiance data, including pressure modes (periods of minutes) and gravity modes (periods of hours to days). (Woodard & Hudson 1983; Woodard 1984; Woodard & Noyes 1985; Frohlich & Delache 1984) Pressure mode oscillations of low degree (L=0,1,2) and orders 15 - 25 have been derived from ACRIM I shutter cycle observations (averages over 32 seconds spaced every 131.072 seconds) as shown in Figure 3.1.3. Peak amplitudes of these '5 minute' oscillations are 3 ppm of the total irradiance signal. Results of 'P-mode' analysis of ACRIM I data have provided new physical insights on the properties of the convection zone and the outer solar core. The most significant of these are: (1) Support for the relativistic interpretation of Mercury perihelion observations; (2) An upper limit to the radial variation of solar rotation of 2.2 times that of the photospheric rate; (3) Coherence times for oscillation modes of 1 - 2 days; (4) A frequency shift of the modes of the results for the 1980 (solar active) and 1984-86 (solar quiet) periods that may be related to the solar cycle luminosity trend. (Woodard 1984)

There are preliminary indications that detectable gravity mode (G- mode) oscillation signatures exist in the ACRIM I results. (Frohlich & Delache 1984) Analysis by one group claims to have isolated G-mode signals in the 10 - 80 uhz frequency range (one day to several hours periodicity). If true, the G-mode signal structure can provide information on the physics of deep solar layers, extending to the solar core. A G-mode periodicity of 29.85 minutes derived by from ACRIM I data supports the weakly interactive massive particle (WIMP) model of the solar core. If this or another 'cool' solar core model is supported by further analysis, it could explain the observational 'neutrino deficit' of 'hot' solar core models.

3.2 Empirical models of TSI variability

Once total irradiance variability on solar active region and sunspot cycle time scales was established, empirical irradiance models were developed to explore the physical causes of the variability and extrapolate the variability to past, and predict future solar cycles. Most models were based on linear regressions between the ACRIM I and/or ERB results and several solar activity indices, such as the Zurich sunspot number, the 10.7 cm. radio flux and the time series of solar emission lines observed in both satellite and ground based experiments.

3.2.1 Active region time scales

Variability on solar active region time scales was the focus of the first models. The total irradiance deficit effect of sunspots, the so-called photometric sunspot

index (PSI), was calculated from the area and contrast of sunspots, taking into account the limb darkening. (Hudson & Willson 1982)

Hoyt and Eddy (1982) developed a model using their sunspot ‘blocking’ function and the Zurich sunspot index to predict the total irradiance variability extending back to 1874. They found that irradiance models based solely on the sunspot ‘blocking’ could explain only about half the total irradiance variation observed by ACRIM I.

The next obvious step was to incorporate faculae into the models. Active region faculae were recognized as significant contributors of excess flux, relative to the undisturbed photosphere. They were considered the probable candidate mechanism of offsetting the energy deficit of sunspots in active regions from early studies of the total irradiance measured by ACRIM I. (Willson et al. 1981, Willson 1984, Chapman 1983) Similar conclusions were derived from UV observations made by the Solar Mesosphere Explorer (SME) mission. (Rottman 1988) Precision ground based photometry of the solar disk has convincingly demonstrated these effects for faculae. (Chapman et al. 1986)

3.2.2 Solar cycle time scales

As the length of the ACRIM I and ERB database extended from the maximum of solar cycle 21 to the minimum marking the end of cycle 21 and the beginning of cycle 22, the interest of modelers shifted to the solar-cycle time scale. The results of models by several investigators indicated that the distributed, faculae-like, 'active network' provides a significant contribution to the total irradiance variation on solar cycle time scales (~ 11 years). (Foukal & Lean 1988, 1990; Willson & Hudson 1988) The active network is thought to be populated by residual faculae from former active regions and/or faculae-like features deriving from general solar magnetic activity. Many of the major features of the irradiance data during the declining phase of solar cycle 21 and at the beginning of cycle 22 were reproduced successfully by linear regression models using the full disk equivalent width of the He I line at 1083 nm, the 'core-to-wing ratio' of the Mg II line and the 10.7 cm radio flux.

3.2.3 Shortcomings of linear regression models

Solar cycle TSI variation is predicted with varying degrees of success by regression models using the precision TSI database and 'proxies' of solar activity, such as the Zurich sunspot number, the 10.7 cm microwave flux, He I 1083 nm flux and the 'core-to-wing ratio' of Mg II. The use of the He I model led to the initial realization of the primary role of faculae and the bright network in the solar cycle TSI variation during the declining phase of solar cycle 21 and the ascending phase of cycle 22. Significant divergences occur between the measured and modeled TSI, however. Of particular concern is the model

underestimates of TSI near the maxima of both solar cycles 21 (1980 - see figure 3.2.1) and 22 (1991), indicative of the lack of understanding of the underlying solar physics responsible for TSI variability, particularly during times of high solar activity. (Willson & Hudson 1988, 1991)

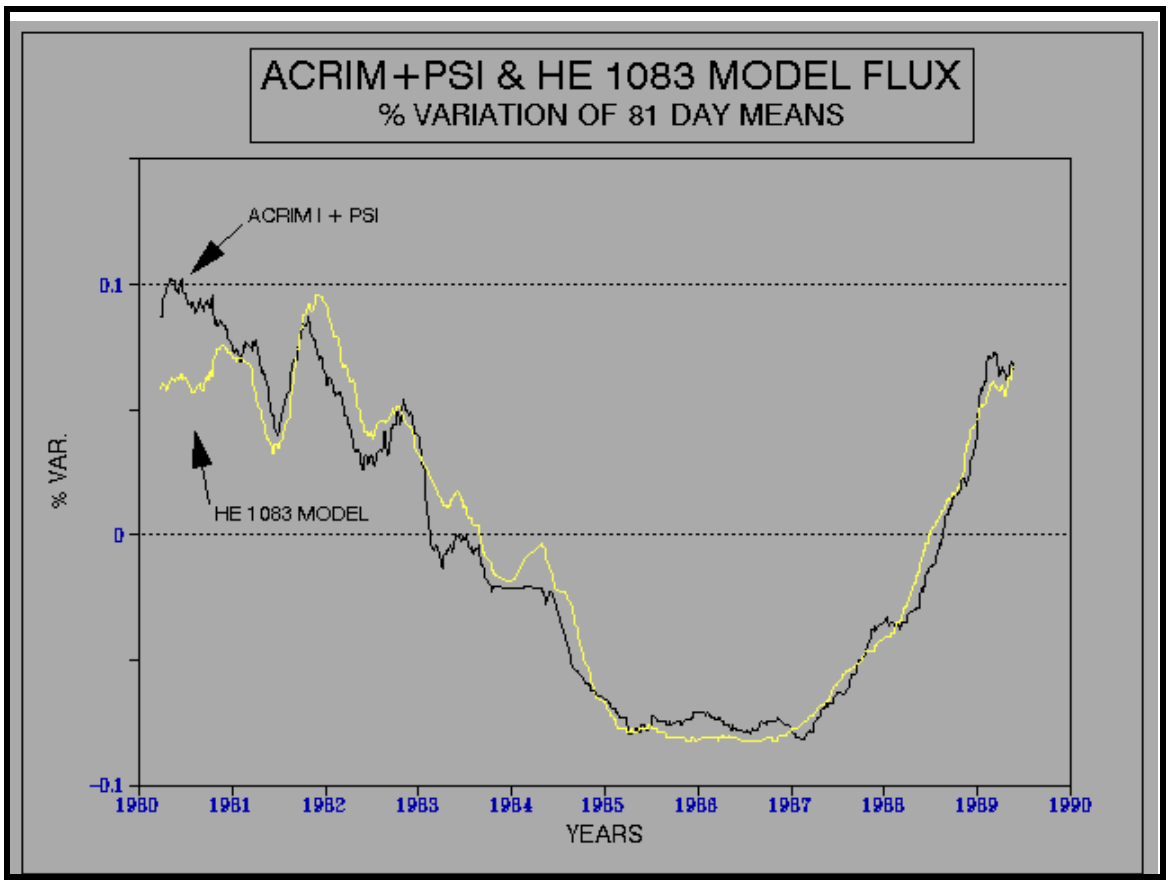

Figure 3.2.1 Comparison of TSI observations by ACRIM I, corrected for PSI, and the predicted TSI of a linear regression model based on the equivalent width of the solar He I line at 1.083 um.

3.2.4 Multivariate spectral analysis

While linear regression models can provide useful insight into the physics of total irradiance variations during part of the solar cycle, multivariate spectral analysis has been shown to be an effective tool in studying the combined effect of various solar phenomena on the TSI. (Frohlich & Pap 1989) Results of multivariate spectral analysis have shown that during the maximum of solar cycle 21 in 1980, sunspots caused most of the power spectral density of ACRIM I's time series. During solar minimum (1984-85) more than 80% of the power spectral density at the average solar rotation period (~ 27 days) was caused by faculae and the active network. Multivariate analysis also shows power spectral

peaks that are not explained by sunspots, faculae or the bright magnetic network near periods of 27 and 9 days, indicating that yet to be discovered solar events are modifying total solar irradiance.

3.3 Constructing the long term Climate TSI database

3.3.1 Total solar irradiance monitoring strategy

The detection of solar luminosity variability during solar cycles 21 and 22 thus far underscores the need to extend the irradiance database indefinitely with maximum precision. There may be other luminosity variabilities with longer periodicities and/or proportionately larger amplitudes that could have significant climatic implications. Subtle trends in the total irradiance of as little as 0.1 % per century could eventually produce the extreme range of climates known to have existed in the past, from warm periods without permanent ice, to the great ice ages. Accumulation of a database capable of detecting such trends will necessarily require the results of many individual solar monitoring experiments. If these experiments last an average of half a decade each, about the maximum that can be expected from today's technology, they will have to be related with a precision smaller than 10 ppm.

A careful measurement strategy will be required to sustain adequate precision for the database since the uncertainty of current satellite instrumentation on an absolute basis is inadequate for this purpose (no better than +/- 0.1 %). An approach must be used that relates successive solar monitoring experiments at a precision level defined by the operation of the instrumentation. Overlapping their flights and comparing of their observations accomplishes this. A relative precision of less than 5 ppm is achievable for the data from overlapped solar monitors with the current state-of-the-art, given sufficient comparison observations. The principal remaining uncertainty for the 'overlap strategy' is the degradation of solar monitor sensors during extended missions. Calibration of degradation using redundant sensors in phased operation can sustain the precision of the long term TSI database at the 10-ppm level.

3.3.2 Relating SMM/ACRIM I and UARS/ACRIM II results

The SMM/ACRIM I and UARS/ACRIM II experiments were originally planned to start the ‘overlap strategy’ through direct in-flight comparisons. However the delay of the UARS launch until 1991 and the termination of the SMM in late 1989 made this impossible. The ACRIM I and ACRIM II databases have been related with useful precision using a 'third party' comparison with the Nimbus7/ERB and NASA ERBS experiments. The daily mean ACRIM I, ACRIM II, ERB and ERBS results were compared for the days on which they each had observations. The results of these comparisons are shown in Table 3.3.1.

The benefit of redundant TSI monitoring experiments is clear, it has preserved the continuity of the TSI database. Without these overlapping comparisons, the relationship of future TSI observations to the past could not be established with precision smaller than the solar cycle variation. From Table 3.3.1 it can be seen that the ratio of ACRIM I/ACRIM II can be established with an uncertainty of 14 ppm using the ERB comparisons, and with 31-ppm uncertainty using ERBS. A mean ACRIM I/ACRIM II ration derived from both ERB and ERBS comparisons, weighted by their uncertainties, is also shown.

These results assume only random errors affect the ratios. This is not the case can be clearly seen in Fig.'s 3.3.1 and 3.3.2 where trends are obvious in the plots of ratios of Nimbus7/ERB and ERBS to ACRIM I and ACRIM II. The causes of systematic differences between ACRIM I & II, ERB and ERBS are not known with certainty but uncorrected sensor degradation, thermal drift effects and solar pointing errors in the ERB and ERBS are highly probable. During the rising activity phase of solar cycle 22, the enhanced high-energy solar fluxes may have accelerated degradation of the ERB and ERBS sensors. Evidence of this can be seen in Fig. 2.2.1.1 where the rate of increase of TSI is lower for these experiments than for ACRIM I during the 1988-1989 period.

Table 3.3.1 Comparisons of SMM/ACRIM I and UARS/ACRIM II with Nimbus7/ERB and ERBS.

Comparisons	Samples	Ratios	Uncertainty
			(Prob. Error)
Nimbus7ERB/ACRIM			
Nimbus7ERB / ACRIM I	2714	1.003138	0.000005
Nimbus7ERB / ACRIM II	368	1.004832	0.000014
ACRIM I / ACRIM II		1.001689	0.000015
ERBS/ACRIM			
ERBS / ACRIM I	138	0.998400	0.000022
ERBS / ACRIM II	221	0.999756	0.000019
ACRIM I / ACRIM II		1.001358	0.000029
Weighted Mean ACRIM I/ACRIM II Ratio		1.001621	0.000013
Nimbus7ERB/ERBS			
ERB/ERBS during ACRIM I (1985-89)	254	1.004833	0.000025
ERB/ERBS during ACRIM II (1991-93)	50	1.005146	0.000031

ERB/ERBS Ratio change		0.000313	

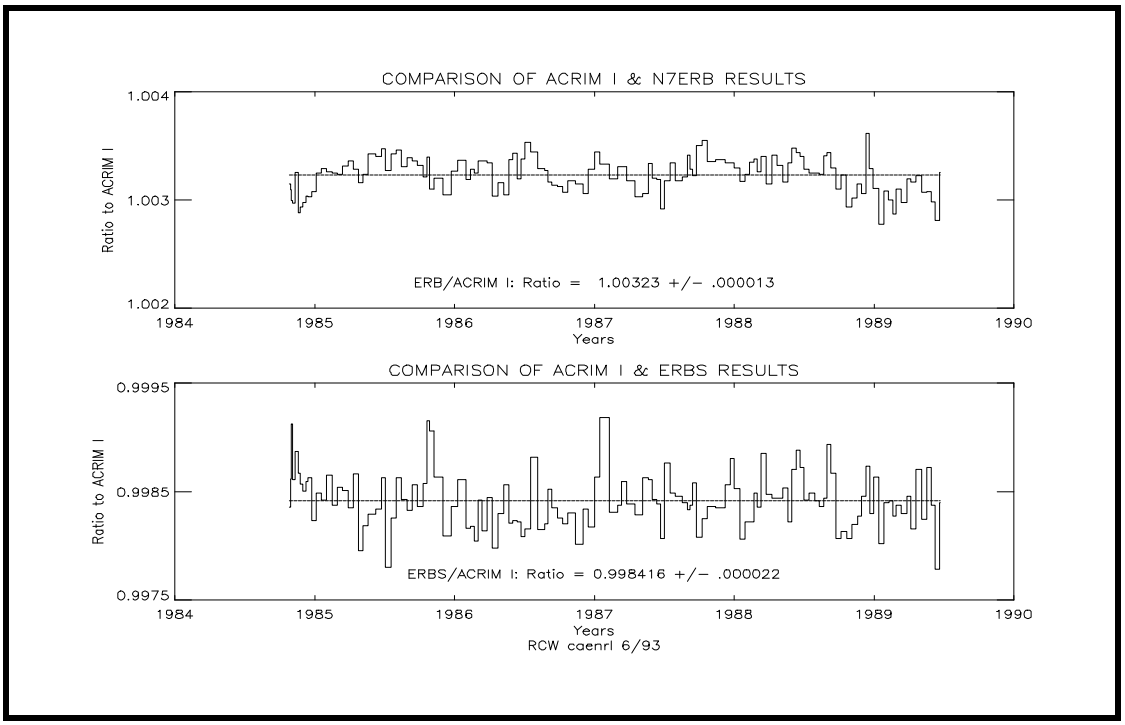

Figure 3.3.1 Comparisons of Nimbus7/ERB and ERBS with SMM/ACRIM I for coincident observation days.

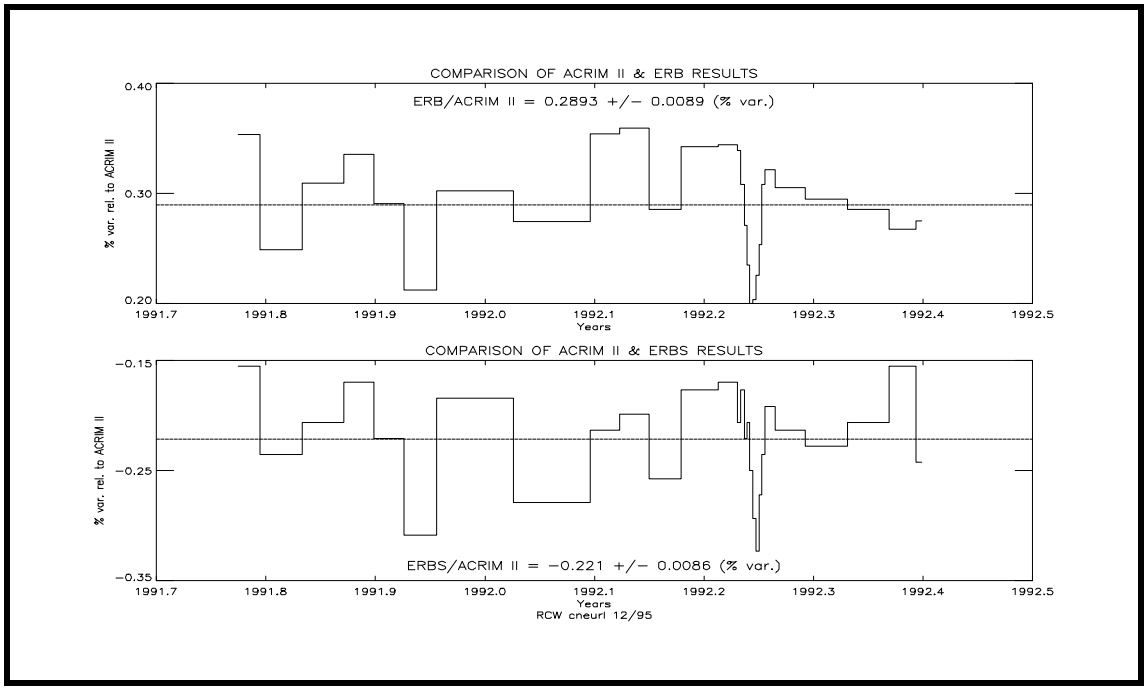

Figure 3.3.2 Comparisons of Nimbus7/ERB and ERBS with SMM/ACRIM I for coincident observation days.

The source of the systematic downward trend of ERB and ERBS ratios to ACRIM II in Fig.'s 3.3.3 and 3.3.4 are likely the effect of uncalibrated degradation of the ERB and ERBS sensors. Degradation of TSI cavity sensors in space is known to be proportional to exposure to solar flux. (Willson 1984) By 1993 ERB had been in orbit more than 14 years and although ERB's solar exposure is only about 10 % of ACRIM's per orbit, degradation should be expected to be a factor in ERB results since it has no degradation calibration capability. Similar considerations would lead one to suspect degradation in the ERBS results as well after more than a decade in space.

The source of the higher order variations is less apparent but likely has causes in the thermal cycling of the ERB and ERBS during the year due to the changing earth-sun distance as well as a host of other possible sources of experimental error peculiar to each experiment. Evidence of ERB and ERBS errors caused by thermal effects and/or solar pointing errors can be observed Fig.'s 3.3.3 and 3.3.4 where the optimum fit to each database is shown with the detrended database. A revision of the ERB results corrected many of the database problems due to pointing errors and thermal drifting, but concluded that residual errors remained. (Hoyt et. al. 1990)

The ACRIM experiments have a redundant sensor degradation calibration capability. ACRIM I's total degradation of 600 ppm of the TSI over its 9.75-year mission was calibrated with a residual uncertainty of 30 ppm. A component of the detailed differences between the four databases is contributed by errors in ACRIM performance as well. By virtue of its more stable spacecraft thermal environment, continuous electrical self-calibration, self-calibration of sensor degradation and precise solar pointing, the contributions are expected to be much smaller than those of ERB and ERBS.

The other significant factor for relating ACRIM I and ACRIM II using ERB and ERBS is the relative uncertainty of the three sets of observation. The standard error of each day's observation for all three sensors is shown as a vertical tic mark through each point in figures 2.2.3a and b. The qualitative differences between the three databases are obvious with the ACRIM I experiment by far the most precise, followed by the ERB and with ERBS significantly less precise. When deriving the relationship between ACRIM I and ACRIM II results using comparisons with other experiments, the quality of the information content in each candidate database must be considered. Clearly the optimum choice here is the Nimbus7/ERB database or a weighted mean of the ERB and ERBS results as shown in Table 3.3.1.

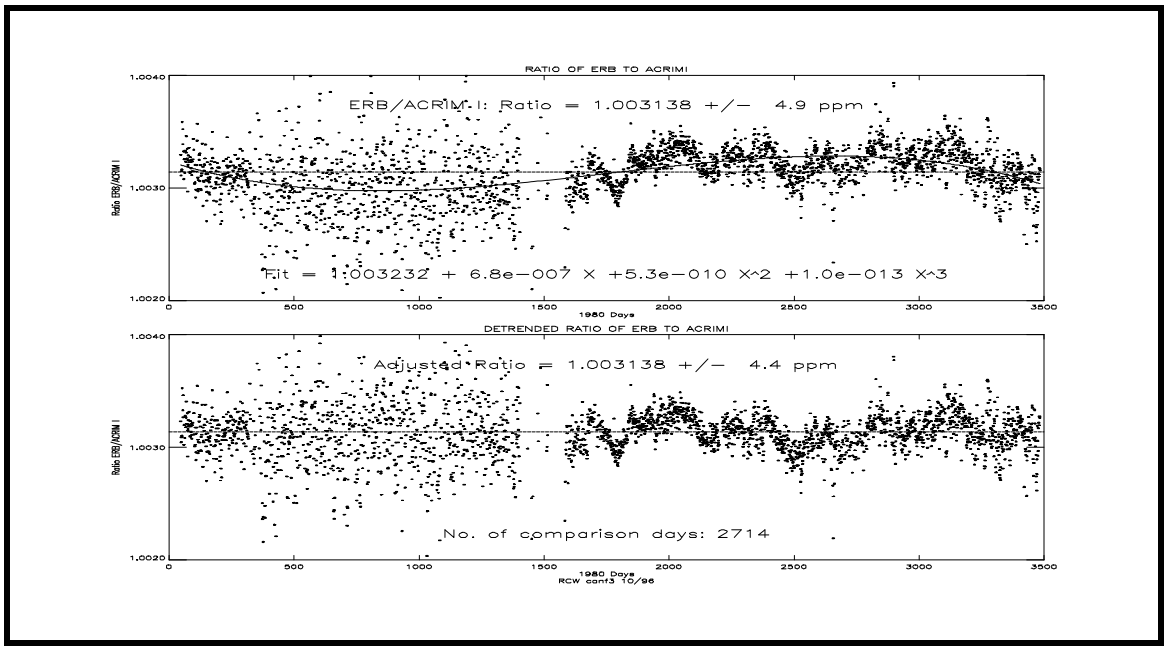

Figure 3.3.3a Best fit and detrended results of Nimbus7/ERB and SMM/ACRIM I comparisons for coincident observation days.

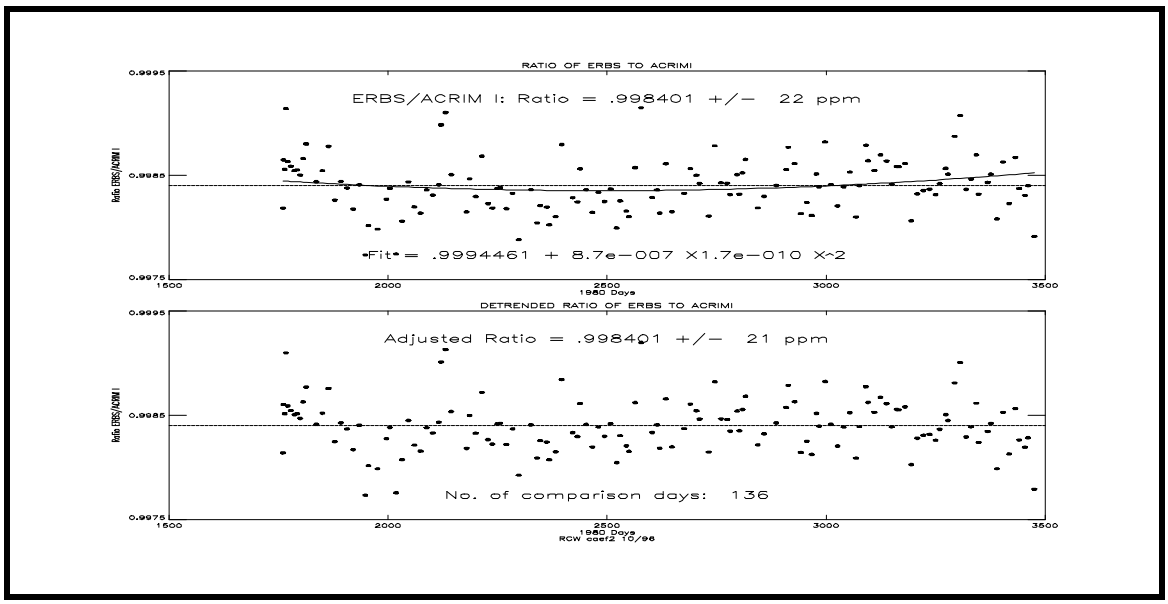

Figure 3.3.3b Best fit and detrended results of ERBS and SMM/ACRIM I comparisons for coincident observation days.

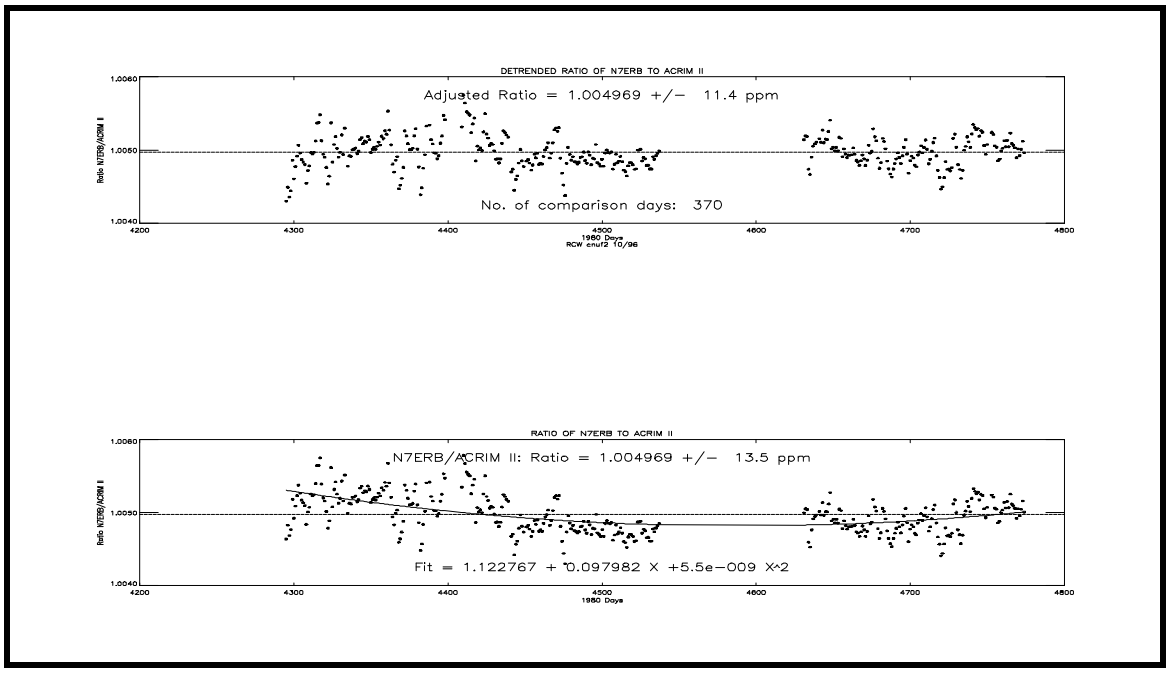

Figure 3.3.4a Best fit and detrended results of Nimbus7/ERB and SMM/ACRIM I comparisons for coincident observation days.

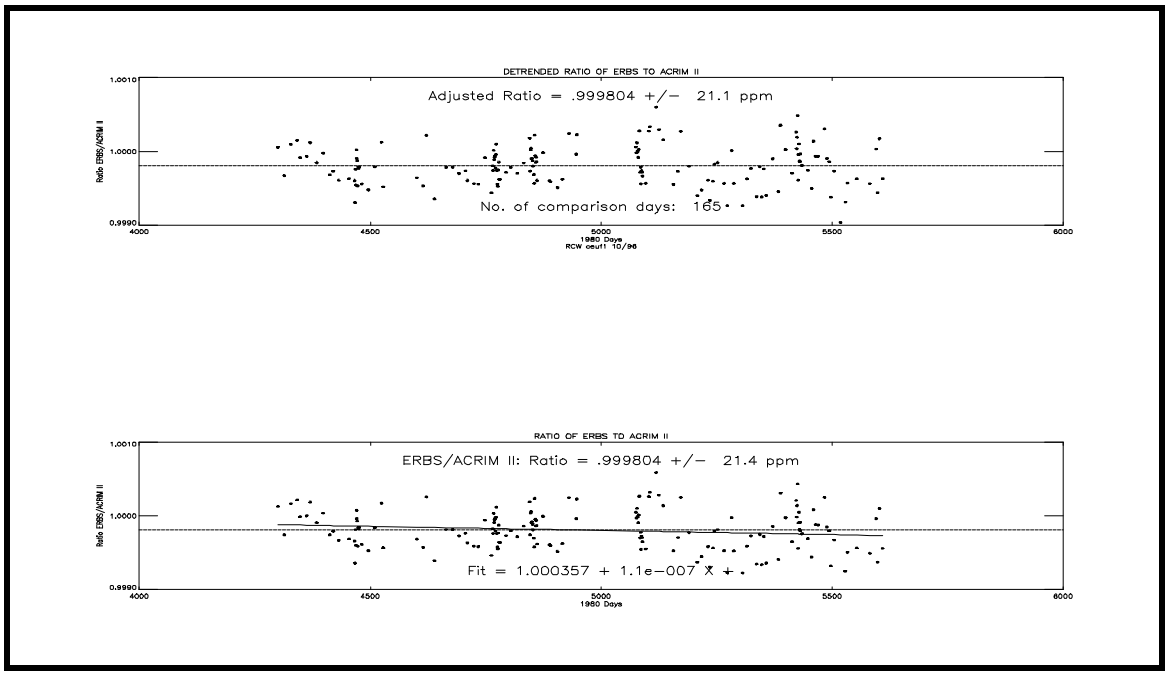

Figure 3.3.4.b Best fit and detrended results of ERBS and SMM/ACRIM II comparisons for coincident observation days.

3.4 EOS/ACRIM Instrument description

3.4.1 Active Cavity Radiometer Sensors

Pyrheliometers have been constructed in various forms, but they all have certain features in common. The heating effect of irradiant flux on a detector is compared with that of electrical power dissipated in a heating element in intimate thermal contact with the detector. An accurate knowledge of the effective absorptance of the detector for the irradiant flux, the area over which the detector is illuminated and the electrical heating power facilitates the accurate measurement of irradiant fluxes on an absolute basis in the International System of Units (SI).

The instrumentation concepts of the Active Cavity Radiometer (ACR) Type IV pyrheliometers are shown in Figure 3.4.1.1. Two right circular conical cavity detectors are thermally connected to the heat sink through their respective thermal impedances. The interiors of the cavities are coated with a specular black paint with high absorptance throughout the solar spectrum. A low temperature coefficient of resistance heater winding is bonded to each cavity, covering the area on the outside of the cavities that corresponds to the area irradiated through the primary aperture on the inside cavity surface. A high temperature coefficient of resistance sensor winding is mounted at the top of each thermal impedance.

The cavity assembly is mounted in its own thermally isolated heat sink module shown in Fig. 3.4.1.2. The primary cavity is irradiated through a precisely machined and accurately measured primary aperture. The detector's external field-of-view is defined by the view-limiting aperture at the top of an extension of the heat sink. The baffles located between the primary aperture and the view limiter prevent scattering from the view limiting assembly walls into the primary aperture. All view limiting components are thermally well connected to the heat sink, which is itself well insulated from the outer case. The sensor Field-of-view of 1.5 degrees accommodates pointing errors of +/- 0.5 degrees without significant compromise of the observations.

3.4.2 Active Cavity Radiometer Operation

Dissipation of a fixed amount of power in each primary cavity will produce a constant temperature difference across the thermal impedance. This difference, transduced by the resistance temperature sensors, is used by an electronic servosystem, which automatically maintains constant cavity power dissipation by controlling the DC voltage supplied to the cavity heater. The primary cavity detector of the ACR is accurately maintained at a slightly higher temperature than the heat sink at all times.

The ACR operates in a shuttered 'differential' mode. A shutter alternately blocks solar radiation from, and admits it to, the primary cavity. The duration of each shuttered state is 65.536 seconds and sampling of the cavity heating power is made every 1.024 sec. In the shutter closed (reference) phase of the measurement, the ACR views its own heat sink and the back of the shutter. Electrical heating provides the necessary power to balance the cavity's conductive and radiative losses and maintains the constant cavity-to-heat-sink temperature difference. When viewing the sun in the shutter open (observation) phase, the power supplied by the electronics automatically decreases by an amount proportional to the solar irradiance of the cavity aperture. Absolute irradiance measurements are derived from the difference in the electrical power supplied to maintain the constant cavity-to-heat-sink temperature difference in the two phases of measurement.

The objective of the differential measurement approach is to remove measurement dependence on the International Practical Temperature Scale. This is successful to the degree that the ‘quasi-equilibrium’ state of the sensor is the same in the two measurement phases.

The settling time of the ACR sensor to 1 least significant bit (lsb) of Analog to Digital (A/D) conversion is less than 30 seconds. To insure well settled out data the last 32 samples of each shutter open interval are averaged to provide the primary data product: the shutter cycle observations.

3.4.3. EOS/ACRIM sensor technology considerations

The EOS/ACRIM experiment, as originally proposed, was to have placed copies of the UARS/ACRIM II instrument on EOS platforms to provide the three five year TSI data segments required by the NASA Announcement of Opportunity (AO-OSSA-1-88). ACRIM was removed from the Chem 1 platform in the 1994 EOS budget re-structuring exercise and made a ‘flight of opportunity’. This led to a search for new implementation approaches that would accommodate our desired late 90’s launch date. The dearth of available satellite platforms capable of carrying the relatively large and heavy ACRIM II instrument led us to consider developing a smaller, lighter ACRIM and combining it with dedicated small satellite technology. The resulting ACRIMSATs would be launched as a series of secondary payloads.

3.4.3.1 Development of smaller ACRIM instruments - two approaches

In the first, and more conservative approach, flight proven ACRIM sensor technology was miniaturized to produce a predictable instrument that could be flown in most small satellite environments and satisfy the experiment science objectives. The second approach involved a more radical miniaturization with little flight heritage. Its purpose was to provide an ACRIM instrument that could be flown in the smallest of the small satellite environments. Both approaches

were to be developed in parallel although most of the effort was expended on the second, since that was where most of the technical challenge lay and the satellite opportunity that seemed most promising at that time was in the smallest size range. Selection of the more suitable of the two approaches was to be made when it became necessary to ‘freeze’ a design and fabricate the first EOS/ACRIM flight instrument.

The first approach is referred to as the Active Cavity Radiometer type VI (ACR VI). It combines three of the flight-tested, dual cavity ACR type IV sensors (each includes a solar and a reference cavity) of the type flown on the SMM/ACRIM I experiment. (See figure 3.4.1.1) The ACR IV sensors have proved to be the best performing dual cavity design. The dual cavities are mounted in sensor module structures of the type employed with the UARS and shuttle ACRIM instruments to provide the thermal stability and isolation essential for state of the art TSI observations. (See figure 3.4.1.2) The ACR VI design reduces the size of the instrument from a 30x45x25 cm. box weighing 30 Kg. to an 18x34 cm. cylinder weighing 12 kg.

The second approach is referred to as the Active Cavity Radiometer type VII (ACR VII). It incorporates four ACR IV type cavities, but not in the dual cavity arrangement. Each of the four single cavities faces the solar viewing direction, thus shortening the instrument. Three provide the required TSI observational redundancy for degradation calibration. The fourth provides the essential non-solar, reference observations (made by the rearward facing cavities in the ACR VI design). The field of view was expanded to increase tolerance for off-sun pointing and further shorten the instrument. The modular sensor mounting was eliminated to minimize instrument weight, but at the cost of reducing the total heat sink mass and exposing the sensors to increased (and uncalibratable) effects of instrument thermal drift. To compensate for the increased thermal drift the development of a more sophisticated ‘Proportional Integrating Differentiating (PID)’ electronic servosystem design was undertaken to decrease the effective sensor thermal time constant. The ACR VII prototype design resulted in a cylindrical instrument with approximate dimensions of 15x20 cm. in size, weighing 5 Kg.

The advantage of the ACR VII design is that it could be flown on a satellite with very limited weight and space resources. But the disadvantages are many including the uncertainty, in the absence of testing, that the design can meet the requirements of the experiment.

The ACR VII incorporates major changes in sensor configuration and electronics in the effort to fit within the space and weight constraints of a very small satellite system. Its larger field of view increases the measurement uncertainties introduced by shuttering assumptions and provides increased sensitivity to stray light within and from without the instrument. The absence of sensor modules significantly increases potential errors caused by thermal drift within the instrument. Thermal drift error cannot be de-convolved from the irradiance signal and is therefore one of the principal drivers of a successful sensor design. The

viability of the ACR VII relies entirely on the successful implementation of the PID servosystem which the sensor research program at JPL has not yet been able to demonstrate.

A variant of the ACR VII referred to as the DBSIM was developed by JPL without the involvement of the PI during 1995. This instrument is essentially identical to the ACR VII with the exception that the reference cavity has been removed. Without the reference cavity, fully independent three-fold redundancy for solar observations cannot be provided and the DBSIM could not adequately calibrate its sensors' degradation. Without this calibration capability, the DBSIM could not meet the science requirements of a TSI monitoring experiment.

3.4.3.2 Selection of the ACR VI instrument design for EOS/ACRIM

The advantages of the ACR VI design are that all of its essential components have been successfully and extensively flight demonstrated in previous ACRIM experiments. It is the least costly approach, requires no prototype testing and is small enough to be flown in virtually any satellite environment capable of supporting TSI monitoring. The ACR VI's ability to produce results we understand and can relate to previous measurements is well understood. This is an important consideration in the 'overlap strategy' to sustain the precision TSI database. The ACR VI could be ready for a late 90's ACRIM experiment and would satisfy our science objectives with minimum technical risk.

The principal reasons for considering the ACR VII design have gone away as other, better satellite flights of opportunity have become available. Additionally, the time and expense of making the considerable modifications required to make it a viable TSI monitoring technology, qualifying it for flight, testing and comparisons with other well understood TSI sensors cannot not be justified. The remedies for the ACR VII sensor configuration problems, principally the wide field of view and omission of the sensor modules, would result in an instrument that is not significantly smaller and lighter than the ACR VI. The PID electronic servosytem, when functional, could reduce the instrument time response (and hence its thermal drift sensitivity) and provide additional resolution in the data. It may be worthwhile using it with an ACR VI or a re-designed ACR VII in the future, but it is not required to meet the objectives of current or future TSI monitoring or EOS/ACRIM science.

The first EOS/ACRIM flight instrument will be similar in design to the instrument developed for the UARS/ACRIM II experiment shown in Fig. 3.4.1.3. Principal differences are: Packaging will be cylindrical instead of rectangular, the sun position sensor will not be included (this ancillary data will be derived from the small satellite's solar pointing sensors), the instrumentation is smaller and lighter overall and the electronics module will be integrated into the sensor assembly. The details of the EOS/ACRIM instrument are listed in Table 2.2.4.

3.5 Theory of Active Cavity Radiometer measurements

3.5.1 Basic properties of the Active Cavity Radiometer (ACR)

From the discussion in section 3.4 we would expect the form of the mathematical abstraction of the radiometer's operations to have the form:

Eq. 3.5.1 $H = K(P_e^r - P_e^o) + E$

Where:

H measured irradiance
K standard detector constant of proportionality
P_e^r cavity electrical heater power in the reference mode
P_e^o cavity electrical heater power in the observation mode
E error terms - departures from quasi-equilibrium assumptions

A major advance in the design of the ACR was implemented in the mid 1970's. The diffuse black absorbing surfaces used by previous ACR's was replaced by specularly reflecting black cavity absorbing surfaces. The advantage of these specular surfaces relative to the diffuse black's used in the ACR's and other radiometer designs up to that time can be seen in eq. 2. The ACR cavity's 30 right circular cone design causes axial rays to undergo 6 reflections before leaving the cavity. The resulting effective cavity absorptance is then the surface reflectance, ρ_s, raised to the power of 6. Although the surface reflectances of specular black coatings is generally ~ 0.9 for TSI, compared to ~ 0.95 for diffuse blacks, the effective cavity absorptance is much higher: typically 0.9999 $\pm$0.0003 for specular coatings and 0.997 $\pm$0.002 for diffuse.

Eq. 3.5.2. $\rho_c = \rho_s^6$

Where:

ρ_c effective cavity absorptance
ρ_s absorptance of cavity surface
6 number of reflections per axial ray

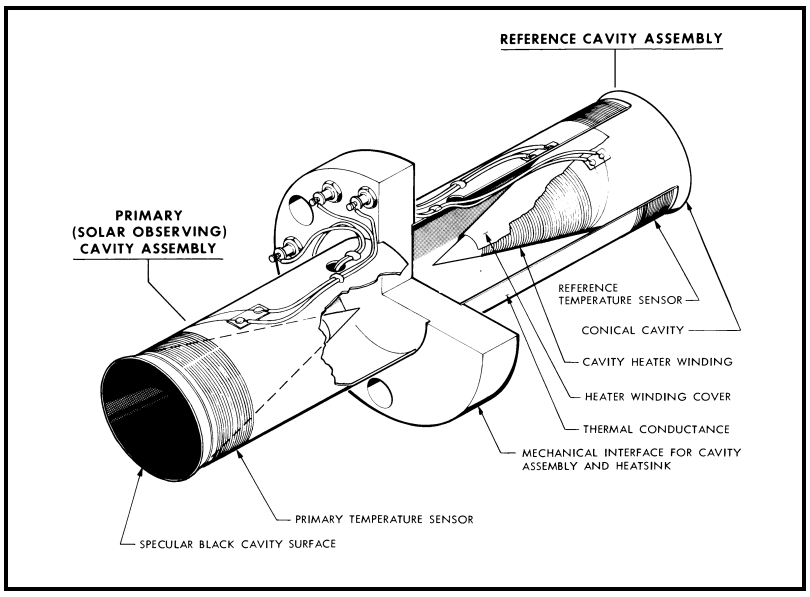

Figure 3.4.1.1 Active Cavity Radiometer dual cavity sensor assembly.

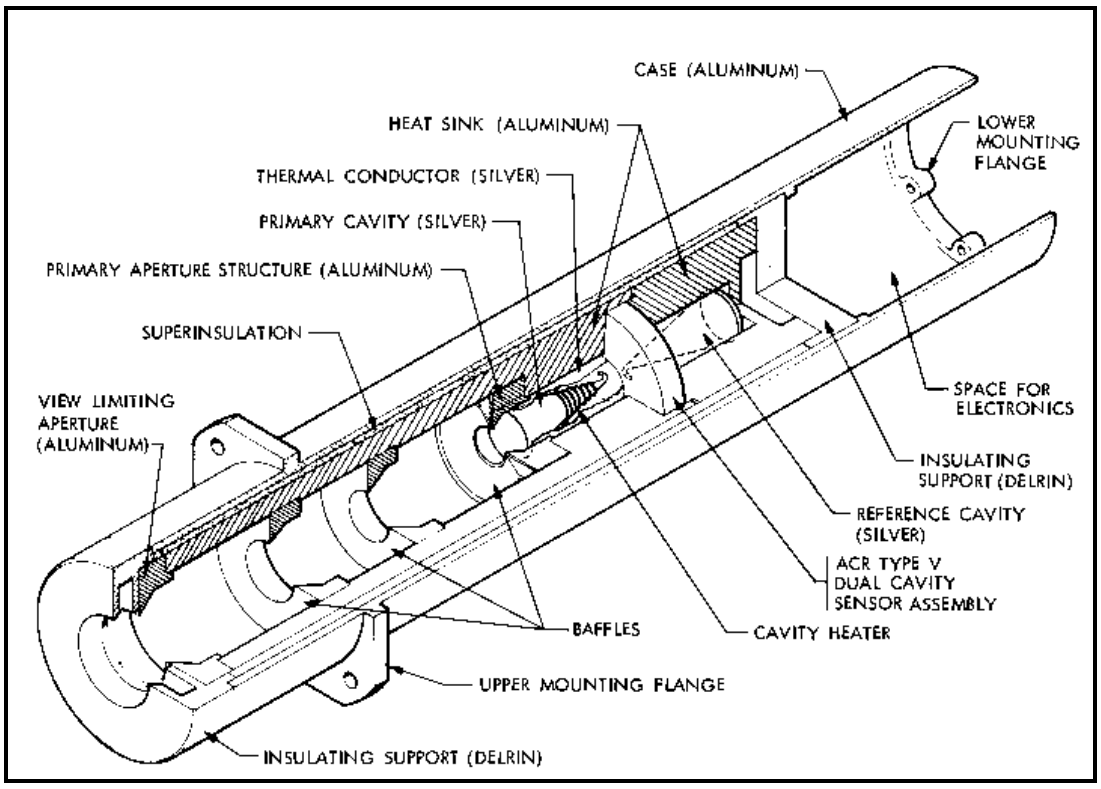

Figure 3.4.1.2 Active Cavity Radiometer modular sensor assembly.

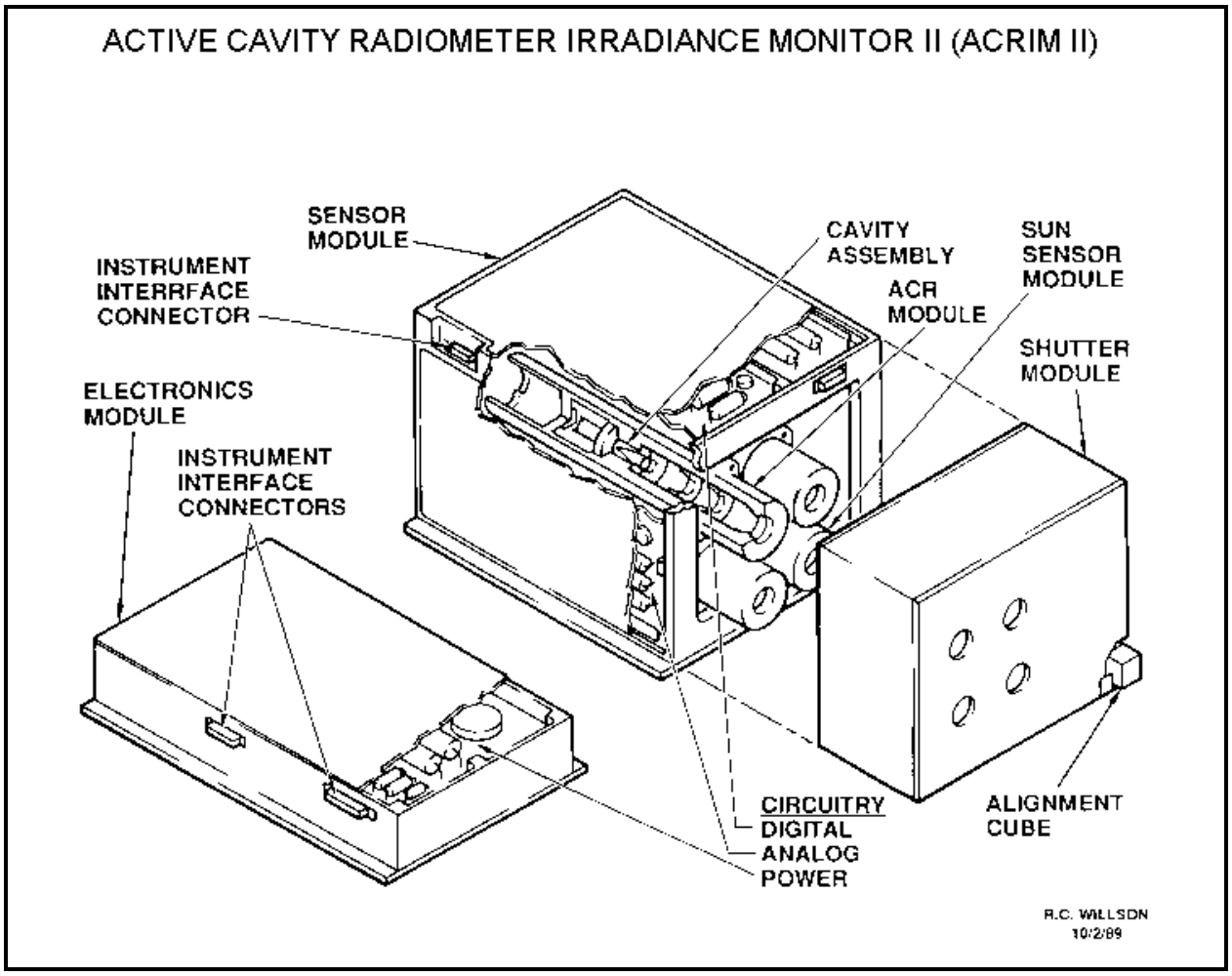

Figure 3.4.1.3 Active Cavity Radiometer Irradiance Monitor instrument for the Upper Atmosphere Research Satellite.

3.5.2 Derivation of the quasi-equilibrium equation:

The starting point in the analysis of the physical properties of the ACR is the concept of viewing the cavity as a thermodynamic entity. We then account for all cavity power inputs and outputs in both the reference (shutter closed) and observation (shutter open) phases of the measurement.

In the reference phase the sums of input and output powers are:

Eq. 3.5.3. $$\sum P_{in}^{r} = P_e^{r} + \sum_j P_{rj}^{r}$$

Eq. 3.5.4. $$\sum P_{out}^{r} = P_c^{r} + C\,[dT/dt]^{r} + \sum_j P_{rcj}^{r} + \sum_k P_{lck}^{r}$$

In the observation phase the sums of input and output powers are:

Eq. 3.5.5. $$\sum P_{in}^{o} = P_e^{o} + A_c H(\alpha_c + \rho\rho_c) + \sum_j P_{rj}^{o}$$

Eq. 3.5.6. $$\sum P_{out}^{o} = P_c^{o} + C\,[dT/dt]^{o} + \sum_j P_{rcj}^{o} + \sum_k P_{lck}^{o}$$

Where:

$\sum_j P_{rj}$	sum of radiative power inputs to cavity
$\sum_j P_{rcj}$	sum of power losses from cavity by radiative processes
P_c	power lost by conduction to the heatsink
C	cavity heat capacity
[dT/dt]	time rate of change of cavity temperature
$\sum_k P_{lck}$	sum of power losses from cavity by electrical lead conduction
α_c	effective cavity absorptance for TSI
ρ	TSI reflectance of cavity's field of view
ρ_c	effective cavity reflectance for TSI

The assumption of quasi-equilibrium requires that the sum of input and output power for the cavity in the reference and observations phases be approximately equal:

Eq. 3.5.7 $$\sum P_{in}^{r} \cong \sum P_{out}^{r}$$ (Reference phase)

Eq. 3.5.8 $$\sum P_{in}^{o} \cong \sum P_{out}^{o}$$ (Observation phase)

Using eq.'s 3.5.2 - 8 we can solve for the electrical heating powers and put the equation in the form of eq. 1. The resulting quasi-equilibrium equation is:

Eq. 3.5.9. $H = [A_c(\alpha_c + \rho\rho_c)]^{-1} \{(P_e^{r} - P_e^{o}) +$ (electrical power term)

$C\,([dT/dt]^{r} - [dT/dt]^{o}) +$ (cavity heat capacity term)

$\sum_j (P_{rcj}^{r} - P_{rcj}^{o}) -$ (radiation from cavity)

$$\sum_{j} (P_{rj}^{r} - P_{rj}^{o}) + \quad \text{(radiation to cavity)}$$

$$(P_{c}^{r} - P_{c}^{o}) + \quad \text{(thermal impedance conductance)}$$

$$\sum_{k} (P_{lck}^{r} - P_{lck}^{o})\} \quad \text{(electrical lead conductance)}$$

3.5.3 Discussion of the quasi-equilibrium equation

The exact forms of the terms in Eq. 3.5.9 are shown in section 3.5.4. A perusal of these demonstrates the important property of ACR operation that except for the electrical power term, the behavior of the ACR is a function of the difference in relative temperature between the cavity and its surrounding fields of view in the two phases of measurement. The essential aspects of ACR IV design are intended to maximize the thermodynamic equivalence of these two phases, which minimizes the effects of the many small temperature dependent terms.

The ACR design attempts to minimize thermal drifting without active controls. Studies of temperature drift effects, using characteristic values of the radiometer parameters and heat transfer modeling based on the above relationships, have been carried out. In the resulting ACR design, the levels of temperature difference errors associated with ACR operation under most conditions are well below the threshold of error defined by other radiometer parameters.

The reduction of the differential temperature terms to negligible values approximates equilibrium conditions and in practical measurements justifies the use of the following equilibrium equation:

Eq. 3.5.10 $$H = [A_c(\alpha_c + \rho\rho_c)]^{-1} \{(P_e^{r} - P_e^{o}) + (P_{r1}^{r} - P_{r1}^{o})]$$

The standard detector constant K of Eq. 3.5.1 is recognized as the first bracket on the right-hand side of Eq. 3.5.10 where the dependence of the constant K on the cavity's primary aperture area A, the cavity absorptance, the cavity reflectance ρ_c and the reflectance of the cavity's field of view ρ (excluding the field of view through the 5-deg view limiter) are shown. The term for the difference of effective radiative temperature seen by the cavity through its view limiting aperture (field of view 1) in the shutter open and closed phases is $(P_{r1}^{r} - P_{r1}^{o})$. The combination of a small field of view and the high reflectance/low emittance shutter surface seen by the cavity makes this term smaller than 0.1%. (Willson 1979) An analytical evaluation of the term, included in all data analysis, reduces the magnitude of its contribution to the measurement uncertainty to less than +0.01 %.

3.5.4 Form of the quasi-equilibrium equation terms

The interaction between the ACR IV primary cavity and its environment is characterized as accurately as possible by describing its power gains and losses due to radiative and conductive processes. The forms of the mathematical descriptions of these interactions are as follows, in reference to Eq. 3.5.9:

3.5.4.1 Cavity heating power term ($P_e^r - P_e^o$):

Eq. 3.5.11 $P_e^r = V^r I^r$

Eq. 3.5.12 $P_e^o = V^o I^o$

Where: V^r, V^o, I^r, I^o are the cavity electrical heater voltages and currents in the shutter closed (reference) and shutter open (observations) phases of the measurement.

3.5.4.2 Cavity heat capacity term C ($[dT/dt]^r - [dT/dt]^o$):

This term represents the net power transferred to or from the heat capacity (C) of the cavity in the two phases of measurement.

3.5.4.3 Radiation from the cavity to its surround $\sum_j (P_{rcj}^r - P_{rcj}^o)$:

Eq. 3.5.13 $\sum_j P_{rcj} = \sum_j \varepsilon_{cj} A_{cj} \sigma T_{cj}^4 F_{cj}$

Where:

ε_{cj} = cavity infrared (IR) emittance to j^{th} field of view (FOV)
A_{cj} = cavity area presented to j^{th} FOV
σ = Stefan-Boltzmann constant
T_{cj}^4 = effective temperature of cavity as seen by j^{th} FOV
F_{cj} = radiative view factor between cavity and j^{th} FOV

3.5.4.4 Radiation to cavity from surround term $\sum_j (P_{rj}^r - P_{rj}^o)$:

Eq. 3.5.14 $\sum_j P_{rjc} = \sum_j \varepsilon_{jc} A_{jc} \sigma T_{jc}^4 F_{jc}$

Where:

ε_{jc} = infrared (IR) emittance of j^{th} field of view (FOV)

A_{jc} = area of j^{th} FOV presented to cavity
T_{jc}^4 = effective temperature of j^{th} FOV as seen by cavity
F_{jc} = radiative view factor between cavity and j^{th} FOV

The 4Π steradian FOV of the cavity has been subdivided into five regions for the analysis of functional relationships between the cavity and its surround:

FOV	Description
1	cavity's view through its view limiting aperture (solar view)
2	cavity's view of the heat sink extension/view limiting assembly
3	cavity's view of underside of primary aperture
4	cavity's view of thermal impedance
5	cavity's view of heat sink

3.5.4.5 Conductance to the heatsink from the cavity ($P_c^r - P_c^o$):

Eq. 3.5.15 $P_c = K_{ti}(T_c - T_{hs})$

Where:

K_{ti} = thermal conductance from cavity to heatsink
T_c = cavity temperature
T_{hs} = heatsink temperature

3.5.4.6 Conductance to heatsink through leads $\sum_k (P_{lck}^r - P_{lck}^o)$:

Eq. 3.5.16 $\sum_k P_{lck} = \sum_k K_{lck} (T_c - T_{hs})$

Where:
K_{ti} = thermal conductance of electrical leads from cavity to heatsink

Characteristic values of the parameters are shown in Table 3.5.1.

Table 3.5.1 ACR Parameters and uncertainties

SYMBOL	UNITS	VALUE	UNCERTAINTY	DESCRIPTION
α_c	-		0.0003	cavity absorptance
$_c$	^{2}		0.00013	area of primary aperture
ρ_c	-			effective cavity reflectance for TSI
ρ	-			reflectance of cavity's FOV for TSI
V^o	volts	3.75	0.00015	cavity heater voltage - shutter open
V^r	volts	7.5	0.00015	cavity heater voltage - shutter closed
I^o	amps	0.008	0.00015	cavity heater current - shutter open
I^r	amps	0.013	0.00015	cavity heater current - shutter closed
K_{ti}	mW/K	100	0.4	thermal impedance conductance
K_{c1}	mW/K	0.1	0.01	cavity electrical lead conductance
σ	mW-cm^{-2}- K^{-4}	5.6697 x 10^{-9}	0.0007 x 10^{-9}	Stefan-Boltzmann constant
C	W-sec-K^{-1}	0.5	0.05	cavity heat capacity
$\varepsilon_{c1, c2, c3}$	-	0.98	0.02	cavity emittance to FOV's 1,2,3
$\varepsilon_{c3, c4}$	-	0.05	0.05	cavity emittance to FOV's 4,5
$A_{c1,c2}$	cm^2	0.5	0.00013	cavity areas seen by FOV's 1,2
A_{c3}	cm^2	1.3	0.13	cavity areas seen by FOV 3
$A_{c4,c5}$	cm^2	5.0	0.2	cavity areas seen by FOV's 4,5
ε_1	-	0.05	0.03	emittance of FOV 1
$\varepsilon_{2,3}$	-	0.95	0.03	emittance of FOV's 2,3
$\varepsilon_{4,5}$	-	0.25	0.1	emittance of FOV's 4,5
T_c	K	300.5	10	cavity temperature
$T_{1,2,3,5}$	K	301	10	temperatures of FOV's 1,2,3,5
T_4	K	300.5	10	temperatures of FOV 4
ΔT_c	K	0.01	-	cavity temperature drift per cycle
ΔT_1	K	10	-	FOV 1 temperature drift per cycle
$\Delta T_{2,3,4,5}$	K			FOV's 2,3,4,5 temp. drift per cycle
F_{c1}	-	8 x 10^{-2}	5 x 10^{-4}	cavity view factor to FOV 1
F_{c2}	-	0.923	6 x 10^{-5}	cavity view factor to FOV 2
F_{c1}	-	0.704	5 x 10^{-2}	cavity view factor to FOV 3
F_{c1}	-	0.8	0.08	cavity view factor to FOV 4
F_{c1}	-	0.2	0.02	cavity view factor to FOV 5

3.6 Uncertainty of ACRIM TSI Measurements

3.6.1 General Considerations

The accuracy with which the ACR defines the absolute radiation scale in SI units can be determined by an error analysis of the complete quasi-equilibrium equation. ACR measurements of irradiance depend only on the measured or computed values of ACR parameters and electrical power measurements. The total ACR uncertainty will be equal to that combination of the parametric uncertainties dictated by the quasi-equilibrium equation.

3.6.2 Root-Mean-Square Uncertainty

The conventional representation of random uncertainty, the standard deviation, will be taken as the most justifiable criterion for specifying the ACR uncertainties. In terms of the standard deviations of the ACR parameters, the uncertainty is then

1. $$U(H) = +/- \{ \sum_i [(\partial H / \partial \xi_i) \, S(\xi_i)]^2 \}^{1/2}$$

Where: U(H) is the SI uncertainty of the measured irradiance H and $S(\xi_i)$ is the SI uncertainty of the ACR instrument parameter ξ_i. For clarity, the results of the error analysis are presented here in graphical form. Figure 3.6.1.1 shows the measurement uncertainty of the ACR IV as a function of irradiance level. The largest single source of uncertainty is that due to measurement of the cavity heater power voltages (VR, VO) at the solar constant level (~1367 W/M2). This is followed in magnitude by the uncertainty in determining the cavity absorptance primary aperture area A and thermal lead conduction effects KI. All other sources of uncertainty are below the 0.01% level at the mean level of TSI during solar cycle 21.

3.6.2 Effects of Temperature Drift

In the discussion following Eq. 3.5.9 it was shown that the many small terms represented by E in Eq. 3.5.1 are functions only of very small differences of the temperature field within the ACR in the two phases of measurement. Thus, the absolute temperature of the instrument need not be known accurately, and, to first order, the contribution to the uncertainty of the measurements depends only on small temperature differences. In developing an ACR system for a particular experimental environment, the design goal is to maintain the effective heatsink temperature change at or below ±0.02 K between successive reference observations. If the drift exceeds this by a factor of 5 or more, the uncertainty due to the many radiation exchange terms begins to increase rapidly, as shown

in Fig. 3.6.1.2. The total rms uncertainty has doubled by ΔT = 0.1 K/measurement cycle and is increasing at a rate of about 1%/K by ΔT= 1 K.

A substantial advantage of the active cavity mode of operation arises from the fact that the effective instrument time constant can be decreased by a factor of about 10 by the action of the electronic servosystem that controls the cavity-to-heatsink temperature difference. This reduces the time required between successive reference observations and hence, the temperature change, by corresponding amounts. The effective time constant of the ACR IV can be less than a second for a solar constant step function producing a settling time of less than 15 sec to the least significant bit level of precision in measurement of cavity heating power.

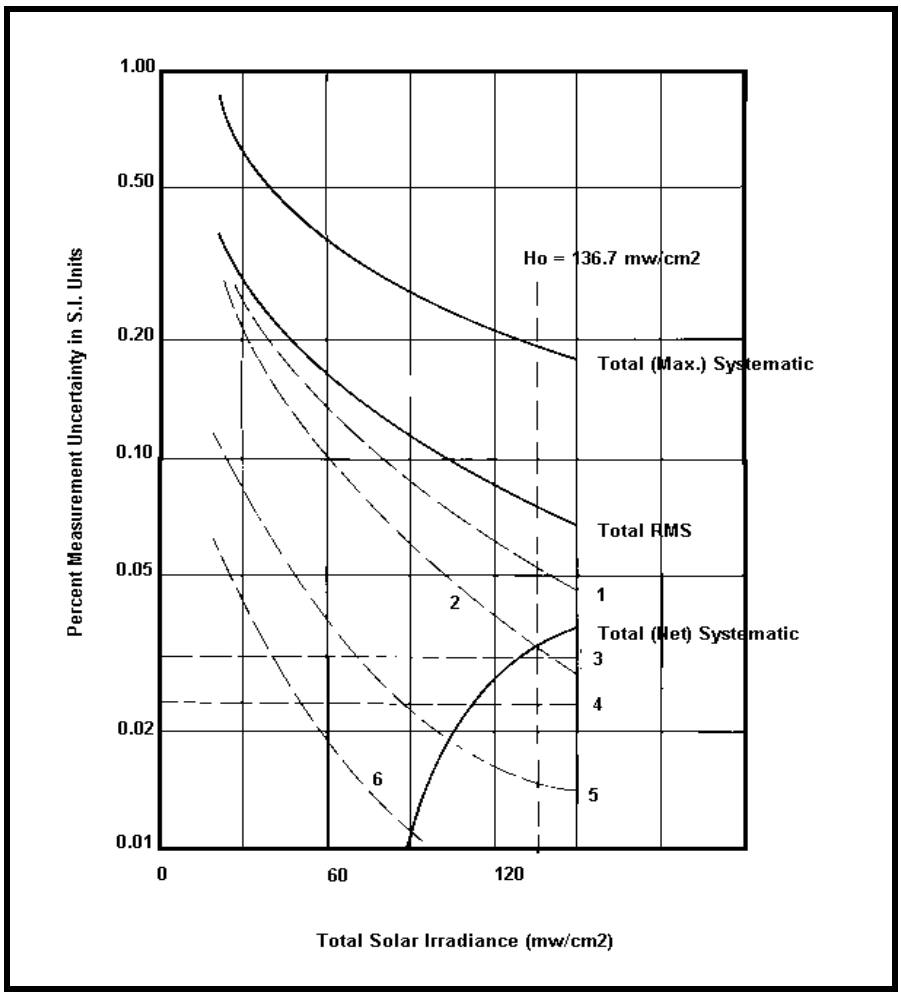

Figure 3.6.1.1 Uncertainty of the Active Cavity Radiometer as a function of irradiance. The contributions to measurement uncertainty of the uncertainties of key parameters are shown as dashed lines: 1 - cavity heater voltage; 2 - area of primary aperture; 3 - cavity absorptance; 4 - conductance of electrical leads; 5 - the area of the cavity surface and 6 - cavity area seen by FOV 4.

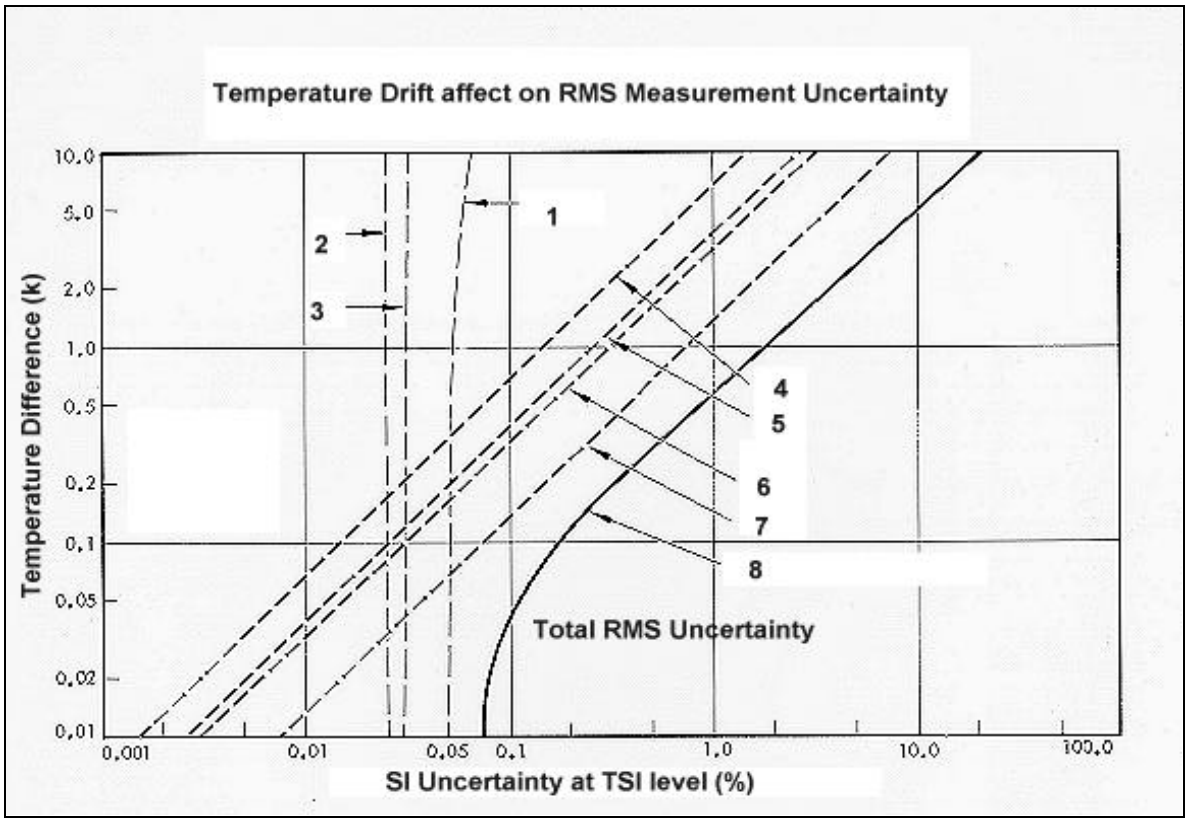

Figure 3.6.1.2 ACR temperature drift affect on uncertainty as a function of temperature difference between successive references phases of measurement (shutter closed). Contributions due to sensor parameters shown as dashed lines: 1 - cavity heater voltages; 2 - area of primary aperture; 3 - cavity absorptance; 4 - cavity area seen by FOV 3; 5 - emittance of 4; 6 - cavity area seen by FOV 2; 7 - cavity area seen by FOV 4; 8 - Total RMS uncertainty.

3.7 Data Plan Summary

3.7.1 Introduction

The EOS/ACRIM experiment is proposed as part of an on-going ACRIM solar irradiance monitoring program of multi-decadal length, comprised of the results of at least four flight experiments including SMM/ACRIM I, UARS/ACRIM II, a shuttle ACR instrument, and a series of three EOS/ACRIM instruments each with a five year mission. The mode of processing data for previous ACRIM experiments has varied from the traditional PI modality of the ACRIM I and shuttle ACR experiments to a more EOS-like approach in the UARS/ACRIM II experiment. The data handling approach of the EOS/ACRIM experiment will conform to the Science Investigator-Led Processing System (SIPS) mode defined by the EOS Project.

3.7.2 EOS/ACRIM data flow

Computer and data communication support instrumentation developed for prior ACRIM experiments is now part of the ACRIM SIPS at the west coast branch of the Center for Climate Systems Research of Columbia University in Coronado, CA. It is operated by the EOS/ACRIM Science team under the direction of the Principal Investigator. All EOS/ACRIM algorithm development, flight data calibration and validation has been conducted using the ACRIM SIPS under the direction of the PI.

Post launch control and management of the EOS/ACRIM Solar Irradiance Monitoring Satellite (ACRIMSAT) small satellite will be the responsibility of the ACRIM flight hardware group of the Jet Propulsion Laboratory (JPL).

3.7.2.1 ECS-ACRIM III SIPS Functional Interface

As summarized in Figure 3.7.2.1, the ACRIM III experiment will be deployed on the ACRIMSAT, a dedicated small satellite. A ground station at the Table Mt. Observatory (TMO) of the Jet Propulsion Laboratory (JPL) will control ACRIMSAT and downlink the data. Level 0 and satellite ephemeris data will be provided via the internet to the Science Team's SIPS in Coronado, CA. Level 0, ancillary data, Level-1, and Level 2 results will be provided to the Langley DAAC by the ACRIM III Science Team SIPS.

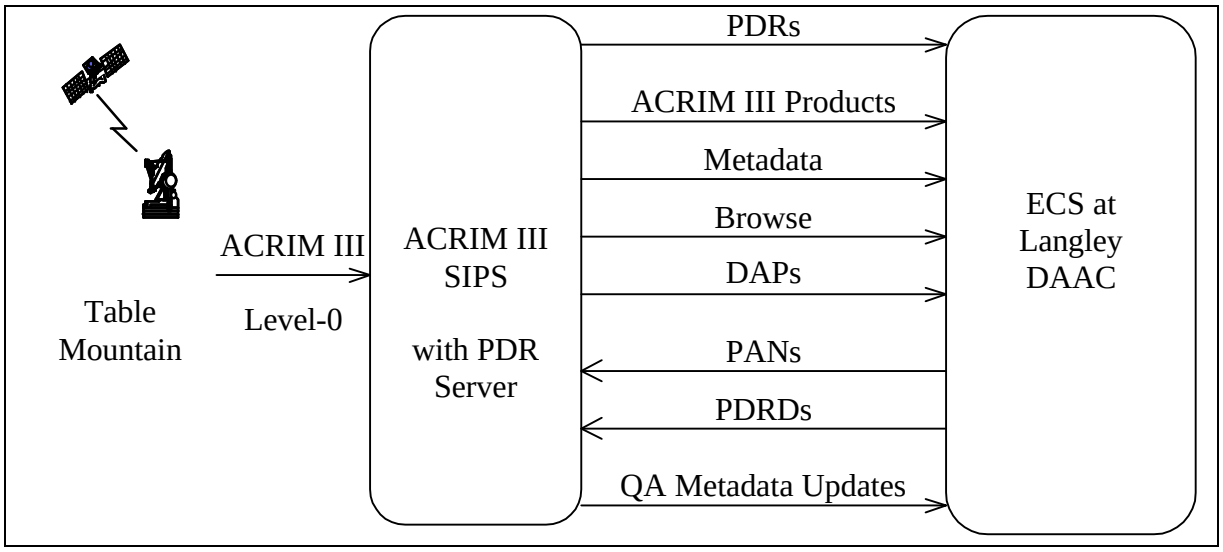

Figure 3.7.2.1 Context Diagram for ECS-ACRIM III SIPS Interface

3.7.2.2 Network Topology

The ACRIM III - ECS network topology is summarized graphically in Figure 3.7.2.2. ACRIM III level-0 and ancillary data and level-1 results will be pulled by the Langley DAAC from an anonymous FTP directory on the ACRIM III SIPS server.

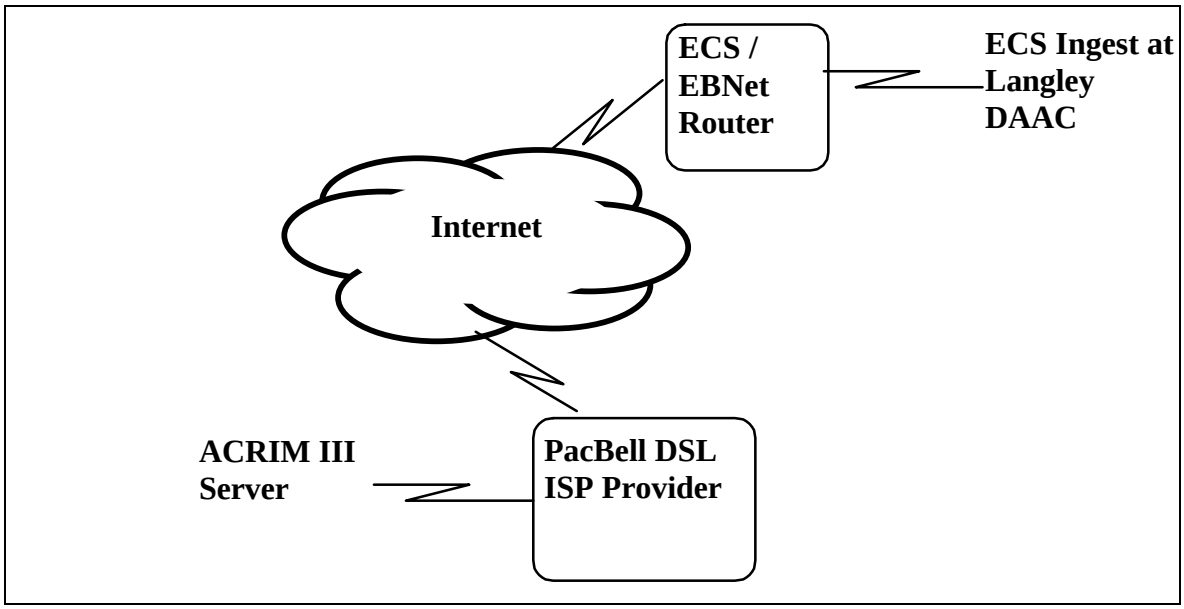

Figure 3.7.2.2 Network Interfaces between ECS and ACRIM III SIPS

3.7.3 ACRIM data types and volumes

3.7.3.1 Standing Order Subscriptions

The ACRIM III SIPS will require no data from the Langley DAAC. The ACRIM III data volume is sufficiently small that the entire dataset will be archived at the ACRIM III production site in addition to the ECS. ACRIM III will perform any reprocessing from their local copy of the raw data and will not require a delivery mechanism for this purpose from the DAAC.

3.7.3.2 Baselined Products according to the SPSO database

The baselined data volumes in Table 3.7.3.2.1 were used to establish the hardware sizes at the ECS archive. These values were estimates in 1996. After development of the ACRIM III system, the actual requirements turned out to be much less. Actual sizes are given in section 3.7.3.3 below.

Table 3.7.3.2.1 EOS Project Science Office Baseline for ACRIM III

Data Rates and Volumes	Rate	Level-0 Volume	Level-1 Volume
ACRIM	1 kps	<2 Mbyte per day	<1 Mbyte per day

3.7.3.3 ACRIM III SIPS products delivered to Langley DAAC

This section lists the Data Types that the ACRIM III SIPS provides to the Langley DAAC using the Polling with Product Delivery Record (PDR) interface functionally specified in Section 4.5, Volume 0 of the ACRIM ICD. The ACRIM III SIPS routinely produces the EOS Standard Data Products specified in Table 3.7.3.3.1 and transfers them to ECS for archiving.

Table 3.7.3.3.1 EOS ACRIM III Standard Data Products

ECS DATA_TYPE ShortName	ECS FILE_TYPE	Collection Description	Granule Size (MBytes)	Transfer Frequency (hours)	Daily Transfer (MBytes
ACR3L0	SCIENCE	ACRIM III Level-0 Data	1.2	24	1.2
ACR3L1SC	HDF	ACRIM III Level-1 Shutter Cycle Data	0.1	24	0.1
ACR3L2OM	HDF	ACRIM III Level-2 Orbital Means Data	0.05	24	0.05
ACR3L2DM	HDF	ACRIM III Level 2 Daily Means Data	0.035	24	0.035
ACR3EPH	SCIENCE	ACRIMSat Ephemeris Data	0.1	24	0.1
				TOTAL	1.485

ACRIM does not use any ancillary data in the production of Standard Data Products. Table 3.7.3.3.2 specifies other products associated with the EOS

Standard Products produced by ACRIM III SIPS and delivered to ECS.

Table 3.7.3.3.2 Other ACRIM III SIPS Products

ECS DATA_TYPE ShortName	ECS FILE_TYPE	Collection Description	Granule Size (MBytes)	Transfer Frequency (hours)	Daily Transfer (MBytes
DAP	DAP	Delivered Algorithm Package	20	each time contents are updated	n/a
BROWSE	BROWSE	Solar Irradiance Graph	10	TBD - less than 1 per day	<10
				TOTAL	<10

3.7.3.4 Delivered Algorithm Package

The delivered algorithm package consists of aA tar file containing the following (as appropriate):

- the source listing of the science processing software,
- software build information,
- software documentation,
- the ACRIM III ATBD (or web address),)
- documentation of all ACRIM III ancillary data and Science Data Products, and
- Data Product User's Guides as appropriate.

3.7.3.5 Browse data

Browse images are delivered as appropriate to an aid outside users in the selection and ordering of ACRIM III Science Data Products. The ACRIM III Browse Image is an image of a graph of solar irradiance verses time.

3.7.3.6 Other Data and Information Transfers

Table 3.7.3.6.1 lists products or information passed from the ACRIM III SIPS in support of this interface. These do not represent particular collections in ECS and they are not ingested through the SIPS interface:

Table 3.7.3.6.1 Other ACRIM III SIPS Transfers

Product or Information	Description
Test data	Sample ACRIM Products
Quality Assurance Metadata	Provided through QA Metadata Update Tool.

3.7.3.7 Test Data

Test data consists of sample Data Products of the data files that ACRIM III will produce. These include a PDR, Data Products with associated .met files, and browse if applicable, and ancillary input files. The purpose is for ECS to get a look at the file contents and provide feedback to ACRIM III of potential items that the ECS can not ingest. This is a hand inspection process.

Corrected Data Products for an Engineering Test. The same sample data products, but of sufficient quality that ECS can perform an automated ingest into the VATC system at ECS. Date Product content does not have to be valid, but the metadata .met file and PDR contents do.

3.8 ACRIM III Data Product Descriptions

The following sections describe the contents, not the format, of the ACRIM III products to be delivered to the Langley DAAC. The actual formats of the Data Products are self-describing in the case of HDF, or are defined in the various documents included in the Delivered Algorithm Package.

3.8.1 Level 0 data

The data from the instrument is comprised of binary cavity shutter heater voltages and currents, sun sensor error signals, internal electronic calibration references, instrument temperatures and a set of engineering data used to monitor satellite and instrument health. These, along with the ACRIMSAT time tags, geocentric coordinates and velocities will be the standard level 0 data.

3.8.2 Level 1 data

The level 1A data product will consist of the experiment data converted to the International System of units (SI).

Level 1B data will be Level 1B corrected for shutter offsets, pointing errors and other minor instrumental effects.

Level 1C data will be the calculated TSI time ordered series in units of watts per square meter for each ACRIM shutter open cycle as observed in-situ by the ACRIM instrument on ACRIMSAT. The basic time resolution will therefore be an average TSI centered on 131.076 second intervals.

3.8.3 Level 2 data

Level 2 data will be Level 1C corrected to 1 Astronomical Unit. The ephemerides for both the ACRIMSAT and Earth orbits will be used to compute correction terms including the effects of the annual earth-sun distance variation (~ +/- 3 %), the ACRIMSAT orbital contribution to the sun-satellite distance variation (~ 100 ppm) and the relativistic effect of the satellite's orbital velocity toward and away from the sun in its orbit (~ 50 ppm). The data will be compiled for orbital and daily means and the time series of daily mean results.

3.9 Data production schedule

Since designation of ACRIM III as a Science Investigation-Led Processing System (SIPS) experiment, extensive interactive planning has occurred with ESDIS personnel. The data processing algorithms, production schedules and archiving plans have been developed in accordance with the ACRIM Interface Control Document (ICD) and Working Agreement with EOSDIS Core System (ECS) and the Operations Agreement between the ACRIM SIPS and the LaRC Distributed Active Archive Center.

Data production software for science data products is in place. ACRIM Earth Science Data Types (ESDT's) have been defined. The Science Data Products toolkit for generation of appropriate metadata has been implemented. The schedule and scenario for provision of level 0, 1 and 2 data products to the LaRC DAAC have are in place (see schedule table below).

Launch is now scheduled for 12/20/99.

The satellite contractor will spend 45 days after launch configuring and checking out the ACRIMSAT satellite. During this period JPL personnel will be trained in the control and operation of ACRIMSAT.

During the initial 45-day configuration period the Science team will have access to ACRIM III data in flight format for the first time. End-to-end data production testing and validation will occur during this period. The efficacy of the data production software has been tested virtually by using a version adapted to process UARS/ACRIM II data.

The scenario for data transfer is in place. Transfer of level 0 data will begin by 2/15/00. Level 0 data will be archived by JPL, the SIPS and the LaRC DAAC.

Satellite operations by the JPL team will begin on or about 2/5/00. The JPL team and the Science team will conduct ACRIM III checkout and initial calibration collaboratively during the February-March 2000 period.

Uncalibrated level 1 and 2 results will be provided for acquisition by the LaRC DAAC during February 2000. Fully calibrated results will be available by June 2000.

ACRIMSAT/ACRIM III Post-Launch Schedule

Dates	OSC	JPL	SIPS
12/20/99	Launch support	Launch support	Launch support
L + 45 days	On-orbit configuration	Learn ACRIMSAT operations	Data processing validation Data transfer validation
2/5/00–3/15/00	Advisory function	ACRIMSAT operations	Initial ACRIM III calibrations Begin transfer of level 0 & uncalibrated results to LaRC DAAC
3/15/00-5/15/00	Advisory function	ACRIMSAT operations	ACRIM III Calibrations Generation of calibrated results Begin transfer of level 0 & calibrated results to LaRC DAAC
6/1/00	Advisory function	ACRIMSAT operations	Routine transfer of calibrated results to LaRC DAAC
6/1/00 →	Advisory function	ACRIMSAT operations	Routine degradation calibrations Routine production of calibrated results Routine transfer of data to LaRC DAAC

4.0 Algorithm Description

4.1 Algorithm design heritage

The ACRIM satellite total solar irradiance monitoring program began with the ACRIM I experiment on the Solar Maximum Mission in 1980. It continued with an ACRIM experiment on Spacelab 1 in 1983 and the ATLAS series of satellite under flights on the space shuttle during 1992 - 1995. The most recent experiment is the ACRIM II on the Upper Atmosphere Research Satellite, launched in 1991 and still on-going. Improvements have been made to the ACR instrumentation over the years but the basic form and function have not changed significantly. The algorithms developed for past ACRIM flight experiments will therefore provide a substantial part of the algorithm for the EOS/ACRIM experiment. The primary differences will be in the detailed layout of the instrument data page and the code and structural formalism required to implement the data reduction software on the EOSDIS.

The EOS/ACRIM instrumentation, as discussed in sections 2 and 3 above, will be similar to that of the UARS/ACRIM II experiment. The UARS data page was allocated a bit rate of 512 bps which included a four fold redundancy in the basic cavity heater power and critical instrument temperatures as well as the on-board engineering data words. Except for A/D conversion and data packet assembly, no data processing will be performed within the satellite instrument. Pyrheliometric instrumentation is highly sensitive to the detailed satellite measurement environment and precise calibration must be performed on the ground with all the relevant measurement parameters available.

4.2 Algorithm mathematical basis

4.2.1 Level 1A data - conversion to the International System of Units (SI)

The binary data page stripped from the downlink telemetry contains cavity heater voltages and currents for the computation of cavity heating power, instrument temperatures for monitoring drift rates, solar pointing information, A/D calibration voltages and currents and ancillary engineering data for monitoring the health and safety of the instrument. A data page is received for every 1.024 seconds of operation. The production of Level 0 data uses binary-to-SI conversion algorithms based on pre-flight calibrations and test results traceable to the National Institute of Standards and Technology (NIST).

4.2.2 Level 1B data - corrections for observational perturbations

The Level 1A data will be corrected for shutter thermal offsets, solar pointing errors, A/D converter calibrations and other minor instrumental effects using the ancillary data contained in the data page.

4.2.3 Level 1C data - the time ordered series of in-situ TSI

The cavity heating voltages and currents are over-sampled in each 1.024 sec. data page. The SI converted data is averaged over the page. The pre and post observation reference phase observations (ref) of cavity heating powers are averaged over the shutter cycle to derive an equivalent projected value for the solar observation phase (obs). Individual obs values are used to compute TSI on 1.024 second intervals during the last 32 pages (1/2) of each shutter open (obs) measurement phase. These results are then averaged to the basic Level 1C result of a shutter cycle TSI time series with a temporal resolution of 131.076 sec.

4.2.4 Level 2 data - correction to 1 Astronomical Unit

Correction to 1 Astronomical Unit requires careful determination of the TSI at a stationary point in the Heliocentric frame of reference. The ephemerides for the ACRIMSAT orbit around the Earth and the Earth's orbit around the sun will be used to compute correction terms for the effects on TSI observations of the earth-sun distance variation (+/- 3.4 % per yr.), the ACRIMSAT orbital contribution to the sun-satellite distance variation (~ 100 ppm) and the relativistic effect of the satellite's orbital velocity toward and away from the sun in its Earth orbit (~ 50 ppm).

4.2.4.1 Correction for the Earth - Sun distance

Ephemerides for the Earth's orbit around the sun will be obtained from the Navigation Systems Section of the Jet Propulsion Laboratory's Engineering and Science Directorate. These tabulations are used to produce the U.S. Nautical Almanac heliocentric Earth coordinates and is being used with the on-going UARS/ACRIM II flight experiment. It is comprised of tabulations of earth-sun distance in Astronomical Unit on four hour centers each day with 8 significant digits of accuracy. Linear interpolation will produce earth-sun distances with less than 0.01 parts per million uncertainty in units of the Astronomical Unit.

4.2.4.2 Correction for ACRIMSAT - Earth distance

The ACRIMSAT orbital ephemerides will be provided for data reduction with position uncertainties of +/- 5 km. and velocity uncertainties of +/- 100 km/sec. relative to a geocentric coordinate system aligned with the 1st point of Aries.

4.2.4.3 Determination of ACRIMSAT - Sun distance

The component of the ACRIMSAT - Earth distance along the Earth - Sun vector is computed to yield the ACRIMSAT - Sun distance at the time of each data page acquisition. The effective TSI at 1 Astronomical Unit is then:

Eq. 4.1 $H_0 = H_i R_{ss}^2$

The ACRIMSAT-sun distance has two components: the heliocentric Earth-sun distance and the geocentric position of ACRIMSAT in its orbit.

The Earth-sun distance is derived from tabulations computed by the Navigation Systems Section of the Jet Propulsion Laboratory's Engineering and Science Directorate. These tabulations produce the Earth-sun distance in units of the Astronomical Unit at four hour intervals with eight significant digits' accuracy.

The orbital motion of ACRIMSAT modulates the ACRIMSAT-sun distance computed from the Earth's orbital ephemerides. The coordinates for the ACRIMSAT ephemerides are based on a geocentric cartesian system whose -x axis is aligned with the first point of Aries at the vernal equinox and whose z axis is aligned with the Earth's axis of rotation.

The orbital ephemerides for ACRIMSAT will be used to derive the ACRIMSAT-sun components of distance and velocity. Computation involves the angle between the 1st point of Aries (Φ) and the inclination of the ecliptic plane (Θ). These relationships are as follows:

Eq. 4.2 $\Phi = 2\Pi(\text{doy} - 80)/365$ or

Eq. 4.3 $\Phi = 2\Pi(\text{doy} - 81)/366$ in leap years.

The transformation of the ACRIMSAT ephemerides to the ACRIMSAT-Earth distance is accomplished by the relationship:

Eq. 4.4 $R_{se} = X_e \cos(\Phi) + Y_e \cos(\Theta) \sin(\Phi) + Z_e \sin(\Theta) \sin(\Phi)$

Where:

X_e, Y_e, Z_e	=	geocentric ACRIMSAT-Earth orbital position or velocity ephemerides
doy	=	day of year
R_{se}	=	geocentric ACRIMSAT-Earth distance along Solar line of sight
Θ	=	$23^o 26' 22''$

4.2.4.4 Relativistic effect of ACRIMSAT-Sun relative velocity

An additional small perturbation of the TSI results derives from a relativistic effect discovered while processing the data of the SMM/ACRIM I experiment. After correcting results to 1 A.U. a residual 2nd order curve was observed in the orbital TSI results that appeared to be dependent on the relative velocity of the satellite and the sun. Correction for the Lorentz 'contraction' of the Satellite-sun relative velocity removed the effect. ACRIM I was the first TSI experiment with a sufficiently low noise level to detect this small effect.

The two most fundamental invariants of the special theory of relativity are the magnitude of the speed of light in a vacuum (c) and the four dimensional distance of any two world points (τ_{12}). The kinematic properties of special relativity that affect solar observations of the sun by satellites with relative velocities are a direct consequence of these invariants.

The properties of special relativity that apply to the TSI observations are expressed by the Lorentz transformation. For simplicity we assume the x axis of ACRIMSAT 's coordinate system is aligned with ACRIM 's line of sight to the sun at time t = 0, the time of a solar observation. The ACRIM-sun distance then depends on their relative velocity along this line-of-sight (LOS) . In the SMM/ACRIM I experiment the maximum relative velocity was less than 10 km/sec. The relative velocity for the EOS/ACRIM will depend on the orbit of insertion which is TBD at this time. The relationship between the stationary earth-sun distance (D_{es}) and the relativistic earth-sun distance (D_{esr}) is:

Eq. 4.5 $$D_{esr} = D_{es} (1 - \beta^2)^{-1/2}$$

Where:

β = v/c
v = relative velocity of ACRIMSAT and sun
c = speed of light

There are two components of the ACRIMSAT-sun relative velocity. The first is the orbital motion of ACRIMSAT, the second and smaller component is the motion of the Earth in its elliptical orbit. Both components are used to correct for the special relativistic effect.

The primary TSI time series produced by the ACRIM experiment will be the shutter cycle time series. This is the mean of observations for the 2nd half of each shutter open solar observation. Orbital mean results will be computed for the study of short term variability by integrating over all shutter cycle data for each orbit. The shutter cycle results will be integrated over mission days to produce the daily means TSI time series

Precise relationships between the EOS/ACRIM time series results and those of

preceding TSI monitor experiments will derived from mutually overlapping sets of observations. The Nimbus7/ERB, ACRIM I, ERBS, UARS/ACRIM II and SOHO/VIRGO observations will be related through a chain of comparison observations to provide the long term TSI database with maximum precision.

4.2.6 Level 3 results - and time series analyses

4.2.6.1 Overview

The ACRIM measurements of total solar irradiance contain information about the variability of solar energy output on all time scales. The principal solar mechanisms of variability that we know about at present are sunspots, faculae, solar cycle, convection, oscillations and flares. From the ACRIM broad-band observation, we hope to be able to study the variability caused by these mechanisms emphasizing the use of the data for predictions of future behavior. Included in this effort will be research into the causes of the variations.

For the purpose of characterizing solar variability as an object of study, the ACRIM data are quite simple: they consist of a single time series of irradiance measurements, together with supporting ephemeris information. Most analyses, especially those on longer time scales, can make use of standard data products and will not require special data preparation. Such analyses are the key ones of interest to the Earth science community, since they describe the variations of solar input on the time scales of weather and climate.

4.2.6.2 Analysis of the Primary Data

The solar irradiance signal contains both narrow-band (e.g., the solar rotation) and broad-band (e.g., the granulation) components. Two basic analysis environments have been used in the past for characterizing such variations: correlation analysis and time-series analysis. The former is more suitable for the longer-term variations, leading to the best representation of any secular term; the latter is most suitable for specific forms of variation with resonant properties.

4.2.6.3 Correlations

In correlation analysis of the solar irradiance signal, we attempt to extract the amplitude of a given physical variation by comparison with specific counterpart data. The sunspot signal gives a typical example. Sunspot umbrae are very dark, relatively speaking, and contribute little to the solar irradiance. Thus a comparison of the total irradiance data with sunspot area, measured independently by using images from solar telescopes, can directly characterize that portion of the irradiance variance "explainable" by the sunspot darkness. At this point the sunspot area measurements become a proxy tool for extending the

estimated total irradiance variation, at least for this component, to times at which direct measures were not available.

The next step in the correlation analysis is to form residuals and to approach the next term in the analysis. The ACRIM-I data on SMM allowed this step to be taken three times: sunspots, faculae, and the "active network" components each could be characterized regressively. The latter arguably provides the main input to the solar-cycle variation of solar total irradiance, which the ACRIM-I data showed to be out of phase with the sunspot area variation itself.

The mathematical tools for this kind of analysis are available in standard statistical packages. By preference our approach will be to implement these by using the IDL analysis language as an interface.

4.2.6.4 Time-series analysis

Fourier transforms and power spectra showed the ACRIM-I data to contain a non-trivial variance fraction in the solar p-modes. These are standing waves trapped in the Sun's interior. They produce a large number of large peaks in the temporal power spectra of total irradiance data, and unresolved peaks from spatially complex modes contribute even more variance in the few-minute band. It has been conjectured, but not established, that g-modes (essentially internal gravity waves, rather than sound-like waves) may also contribute on longer time scales. New tools, specifically wavelet analysis, are now available for this analyzing non-stationary time series of this kind.

4.2.6.5 Special Analyses

Our ability to understand subtle kinds of variation in the ACRIM data will depend upon analysis of the raw data in the context of the measurement itself. An example of this was the discovery of the relativistic perturbation of the ACRIM-I data, caused by spacecraft motion; this effect could easily be measured and removed. We expect that the EOS/ACRIM data will show subtle effects due to spacecraft parameters such as pointing, location, temperature distribution, etc.; because the instrument design specifically eliminates all such effects to first order, these environmental variations will always be small. Nevertheless it will be prudent to characterize them fully, and this will require full access to the spacecraft housekeeping and ephemeris data as well as to the raw ACRIM sensor readings.

4.2.6.6 Solar Secular Variation

The critical output of this measurement program will not be available for many years, over a time scale exceeding that of the 11-year solar cycle. This is the assessment of the amplitude of any secular variation in total energy output from

the Sun. The basic procedure consists of characterizing the time series of residuals against model fits, as sketched below.

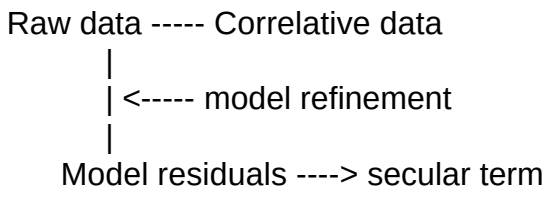

We believe, based upon the present observations, that an intercomparison of ACRIM data between two solar minima will identify a secular term if it exists. This is a sufficiently long time base for such a determination, if and only if the following observational criteria are met:

(a) there must be overlapping data sets, from orbit, of sufficient quality for intercalibration;

(b) these data sets must have internal degradation control, as with the ACRIM design, to permit precise intercalibration.

4.3 Calibration

Calibration of the TSI measurements of the ACRIM instruments is a metrological and theoretical task. The ACR sensors are highly accurate and precise definers of the radiation scale at the TSI level of irradiance. Only narrow wavelength sources in the laboratory can make as accurate definitions of the irradiance scale in SI units.

4.3.1 Metrology of the ACR measurements

The principal factors that determine the accuracy with which the ACR sensors define the TSI in SI units are the cavity heater power measurements, the area of the primary apertures, the absorptance of the cavity for TSI and the thermal conductance of electrical leads. The cavity heater power measurements, primary aperture areas and cavity absorptances are traceable to NIST. The conductance of the leads is modeled using the thermal properties of the materials and their geometry. The combination of uncertainties produced by all the factors affecting the TSI measurement uncertainty is assessed using models based on the discussion of section 3.5 above.

Direct comparisons will be conducted between EOS/ACRIM ACR sensors and the suite of historical TSI sensors maintained at the JPL's Table Mtn. Solar Test site. This will provide relationships between the EOS ACR sensors and previous

ACR sensors flown on the SMM/ACRIM I, UARS/ACRIM II and shuttle Spacelab 1 and ATLAS experiments that will be useful in assessing the readiness for flight of the EOS/ACRIM instrumentation. The comparison precision accessible in these tests is insufficient for relating their flight observations and are not an alternative to the flight experiment 'overlap strategy'.

4.3.2 Theoretical analysis of ACR calibration

Using the quasi-equilibrium equation developed in section 3.5 above, models will be constructed to evaluate the impact of specific design features of the EOS/ACRIM sensors on the overall accuracy and precision of their TSI measurements. Fig. 3.6.1.1 represents the results of one such parametric analysis. When the ACRIMSAT design and orbit are defined, the in-flight environmental factors affecting accuracy and precision will be incorporated into the models.

4.3.3 In-flight calibrations

One of the most important factors affecting the viability of the long term TSI database is the ability to calibrate degradation of the flight sensors of a solar monitoring experiment. The SMM/ACRIM I experiment pioneered this important capability by flying multiple (3), redundant ACR sensors. One ACR is utilized in routine solar monitoring, making observations at every opportunity. The second ACR is used to calibrate the degradation of the first by conducting monthly solar comparison observations. The third ACR is used infrequently to calibrate the first two. It was discovered early in the SMM/ACRIM I experiment that after some initial rapid degradation caused by exposure to the flight environment a solar exposure dependent degradation of the cavity absorptance occurs. By shielding the 2^{nd} and 3^{rd} ACR sensors from the sun most of the time, highly precise calibration of the degradation of the 1^{st} (monitoring) cavity sensor was achievable. This procedure will be employed with the EOS/ACRIM experiment with monthly and tri-monthly comparisons using the 2^{nd} and 3^{rd} ACR's, respectively.

4.4 Validation

The experience of the EOS/ACRIM science team with the SMM/ACRIM I, UARS/ACRIM II and shuttle ACRIM experiments demonstrated repeatedly that two identical days of data are never acquired. Validation will be required on 100 % of the raw data produced by EOS/ACRIM to guarantee results that will be useful for the most demanding applications of the TSI database. Validation will be conducted using the ACRIM SCF.

4.4.1 Validation of Level 0 data

The dual path available for the raw data provides access to both the DAAC and the EOS/ACRIM SCF. At the SCF level 0 data will be scrutinized for consistency with anticipated size and content for each day's data. Departures from normality will trigger an analysis to determine quality, continuity and size of the data available for each day. Changes from normal data flow that require modification of the data processing path will be flagged and the modifications indicated will be identified.

4.4.2 Validation of Level 1 data

The Level 1A data corrections for shutter thermal offsets, solar pointing errors, A/D converter calibrations and other perturbations of instrument performance or properties will be monitored for changes in instrument sensitivity to these parameters and for out of boundary values.

The SI converted data is averaged over the ACRIM data 'page'. The pre and post observation reference phase observations (ref) of cavity heating powers are averaged over the shutter cycle to derive an equivalent projected value for the solar observation phase (obs). These averages will be scrutinized for erroneous results caused by data drop-outs or bit errors.

4.4.3 Validation of Level 2 data

Correction of the TSI to a stationary point in the Heliocentric frame of reference provides the top level discriminator for quality and correctness of the data. Comparisons with predicted solar cycle and solar activity TSI trends will be made to flag potentially erroneous data.

4.5 Quality control

Software quality control will use feedback from the calibration and validation activities. Upgrades to data processing software will derive from indicated changes in the assumptions regarding data flow, ACRIM performance and experimentally determined degradation.

Level 2 and 3 results produced by the version of the ACRIM data reduction software resident on the DAAC will be compared with the validated results produced by the SCF for each day's data. Divergences will be addressed and processing software corrections made where required. Updated software versions will be provided to the DAAC.

5.0 Response to the March 1997 ACRIM III ATBD review's Published Recommendations and General Comments

Richard C. Willson
Principal Investigator – ACRIM Experiments
12/15/99

On 11 to 13 March 1997, there was a first panel review of the Algorithm Theoretical Basis Documents (ATBDs) for the science associated with some of the instruments primarily associated with the PM-1 platform of the NASA Earth Observing. In addition the DAO and ACRIM presented their ATBD's. The following is ACRIM's update to the ATBD and response to weaknesses, recommendations and general comments raised by the review panel in their final report published 10/97.

Response to Executive Summary of Review Panel

Comments on ACRIM

- **capable team that is too small and too scattered**

  The ACRIM III Science Team has been enlarged to include Dr. James Hansen (NASA/GISS) in the climate modeling area, and Dr. Alex Mordvinov (Inst. Of Solar-Terrestrial Physics, Russian Academy of Sciences) in the solar physics area. Dr. Hugh Hudson (UCSD) has continued as a Co-I in the solar physics area. While the team is geographically scattered, this presents no significant problems in the age of the internet. The proximity of the SIPS in Coronado, CA to JPL has facilitated an adequate level of collaboration on ACRIM instrument-related issues.

- **these instruments have a long history of providing useful information**

  The ACRIM III instrument should be the most precise and accurate of the ACRIM series. The design life of 5 years should provide the 1st of three segments of EOS TSI results with state-of-the-art precision.

- **the key to long term use is overlap of successive instruments in the absence of absolute calibration; both should be pursued as much as possible, and hence there should be an active campaign to characterize precision of measurements and their long term drift**

  The ACRIM III instrument will employ the same 3-channel redundancy successfully used by previous ACRIM's to calibrate sensor degradation in the space environment. The UARS/ACRIM II experiment is functioning well at the time of ACRIMSAT/ACRIM III launch. There should be years of overlapping results to connect the ACRIM III results with the previous TSI database at maximum precision.

- **more collaboration with other groups should be fostered to enlarge this small investigator group and to ensure continuity of the data bases well into the future; linkages with Global Information Systems are encouraged**

  The additional Co-Investigators have added collaboration with two important groups of researchers in the climate and solar physics areas. Data and results will be posted promptly on the ACRIM.com experiment website and archived at the LaRC DAAC.

Response to 'Weaknesses':

'there needs to be more description of how measurement precision will be differentiated from high-frequency TSI variability'

The distinction between contributions of inherent ACRIM precision uncertainties and intrinsic solar noise to the apparent uncertainty of TSI observations are difficult to make using solar data. The contributions of short term TSI variability are inextricably convolved with the sensors' response functions. Time frequency analysis of ACRIM performance both with and without the sun could provide insight into sensor characteristics that might be useful in discriminating non-solar variations. The saving feature, however, is that ACRIM sensors are sufficiently slow that perturbation by frequencies shorter than a few seconds will be heavily attenuated.

'Scrutinizing the data is not adequate for detection of erroneous results (i.e., separation of the TSI information from the total measurement noise).'

Detection of erroneous results is complicated by a high probability of occurrences of atypical, short-term solar TSI emissions. The review (or scrutiny) of results that appear atypical or unexpected, using solar activity proxy data (such as Ca II, Mg II core-to-wing ratio and flare observations) are of limited use in detecting erroneous results because their observations are much less precise than the TSI measurements and their relationships to TSI are not well understood on a quantitative basis. Pre-defined algorithms that would discriminate against atypical data based on noise and sampling theory would not reliably accommodate real variances in TSI. Detection of erroneous results must be handled on a case-by-case basis, using whatever observations and theoretical tools are available for the purpose.

'It is important that the different measurement corrections to be applied not only be identified (e.g., shutter thermal effects, cavity heating power, etc.) but that some detail on how these corrections are applied, also be discussed'

The detail of how corrections are applied was explicitly shown in the ATBD instrumentation theory section (error analysis). Specific software coding of the application of corrections to observations, whether arising from instrument variabilities or orbital ephemerides, has been developed as part of the ACRIM data processing software activity and will be part of the delivered algorithm package.

ACRIM III has been designated as a Science Investigation-Led Processing System (SIPS) experiment. The data processing algorithms and archiving approach have been developed in accordance with the Interface Control Document (ICD) between the EOSDIS Core System (ECS) and the ACRIM SIPS (Vol.'s 0 and 1), the Working Agreement between ACRIM SIPS and the ECS and the Operations Agreement between the ACRIM SIPS and the LaRC Distributed Active Archive Center.

Response to Recommendations and General Comments'

'Could a set of ACR's be flown on future ATLAS-type missions and be used for ground and flight test comparisons for both measurement precision and relative accuracy of the EOS/ACRIM observations?'

A properly configured ACRIM shuttle payload could provide useful information on the accuracy and precision of satellite TSI monitors. The accuracy and precision of such 'under flights' was degraded in previous ACRIM shuttle experiments (Spacelab 1 and ATLAS 1,2 & 3) by contamination during the payload integration but still retained a flight-to-flight precision of 200 ppm. This is an order of magnitude smaller than the 'absolute accuracy' of ambient temperature TSI radiometers. With our knowledge of the contamination problem flight-to-flight precisions of less than 100 ppm should be achievable. This could provide an important backup for the long term TSI climate database.

> A more promising approach currently being explored is to deploy ACRIM instruments on the International Space Station on a rotating basis. Following pre-flight comparisons at the JPL Table Mtn. Observatory (TMO), they would be swapped annually and returned to TMO for post-flight comparisons with reference sensors to maintain the thread of in-flight comparisons. This approach could provide 50-ppm long-term precision for the long term TSI climate database. The duration of deployment would provide more data than shuttle flights, reducing the statistical noise of comparisons with free-flying satellite TSI monitors.

'Since the use of ERB-type overlap observations does not completely satisfy the quantitative problem of measurement continuity, further efforts need to be made to verify both relative and absolute accuracy of the results.'

The optimum approach to providing the long-term climate TSI database with the required precision is implementation of an 'overlap strategy' using overlapping deployment of TSI flight experiments. This was the approach presented in the ATBD.

Flight TSI sensors demonstrably capable of defining the radiation scale for total solar flux with 0.01 % (100 ppm) absolute uncertainty are required to provide useful additional information for the TSI climate database. This capability has not yet been demonstrated. TSI sensors operating significantly above the temperature of liquid He are fundamentally constrained to no less than 1000 ppm 'absolute' uncertainty.

The overlap strategy has a demonstrated capability for maintaining TSI precision of better than 50 ppm per decade. It is not clear what, if any, useful role 'absolute accuracy' will play in conserving the long term TSI database.

'However, there is no schedule indicated (in the ATBD) for when the data at all levels will be processed and when Level-3 data would be released. This was understandably of concern to a number of reviewers. How the data will be retrieved, processed, verified, and distributed needs to be explained in more detail than is contained in the document.

The original version of the ATBD was developed prior to the designation of the ACRIM III experiment as a SIPS task. The schedule and modality of production of data products was unsettled at the time of the review, other than that a timely approach in accord with NASA data policy was assumed.

Since designation of ACRIM III as a Science Investigation-Led Processing System (SIPS) experiment, extensive interactive planning has occurred with ESDIS personnel. The data processing algorithms, production schedules and archiving plans have been developed in accordance with the ACRIM Interface Control Document (ICD) and Working Agreement with EOSDIS Core System (ECS) and the Operations Agreement between the ACRIM SIPS and the LaRC Distributed Active Archive Center.

Data production software for science data products is in place. ACRIM Earth Science Data Types (ESDT's) have been defined. The Science Data Products toolkit for generation of appropriate metadata has been implemented. The schedule and scenario for provision of level 0, 1 and 2 data products to the LaRC DAAC have are in place (see schedule table below).

Schedule:

Launch is now scheduled for 12/20/99.

The satellite contractor will spend 45 days after launch configuring and checking out the ACRIMSAT satellite. During this period JPL personnel will be trained in the control and operation of ACRIMSAT.

During the initial 45-day configuration period the Science team will have access to ACRIM III data in flight format for the first time. End-to-end data production testing and validation will occur during this period. The efficacy of the data production software has been tested virtually by using a version adapted to process UARS/ACRIM II data.

The scenario for data transfer is in place. Transfer of level 0 data will begin by 2/15/00. Level 0 data will be archived by JPL, the SIPS and the LaRC DAAC.

Satellite operations by the JPL team will begin on or about 2/5/00. The JPL team and the Science team will conduct ACRIM III checkout and initial calibration collaboratively during the February-March 2000 period.

Uncalibrated level 1 and 2 results will be provided for acquisition by the LaRC DAAC during February 2000. Fully calibrated results will be available by June 2000.

ACRIMSAT/ACRIM III Post-Launch Schedule

Dates	OSC	JPL	SIPS
12/20/99	Launch support	Launch support	Launch support
L + 45 days	On-orbit configuration	Learn ACRIMSAT operations	Data processing validation Data transfer validation
2/5/00–3/15/00	Advisory function	ACRIMSAT operations	Initial ACRIM III calibrations Begin transfer of level 0 & uncalibrated results to LaRC DAAC
3/15/00-5/15/00	Advisory function	ACRIMSAT operations	ACRIM III Calibrations Generation of calibrated results Begin transfer of level 0 & calibrated results to LaRC DAAC
6/1/00	Advisory function	ACRIMSAT operations	Routine transfer of calibrated results to LaRC DAAC
6/1/00 →	Advisory function	ACRIMSAT operations	Routine degradation calibrations Routine production of calibrated results Routine transfer of data to LaRC DAAC

'What specific role will the Co-Is play in these activities? It would be helpful if an approximate timeline were outlined for when the finished product would be available (4 to 6 months after launch?) to the relative/relevant scientific community.'

Co-I Activity is limited to specification of data product formats. The Co-I's are primarily users of ACRIM data products and are not involved in their production.

The timeline for data production, calibration and archiving is in the Post-Launch Schedule table above.

'The ACRIM results released so far have provided important data for application to various general circulation studies of climate change. The usefulness of this information could be enhanced if, as has been suggested, a more formal arrangement than yet indicated would be developed involving relevant colleagues at GISS and, hopefully, graduate students at Columbia University.'

In direct response to this recommendation we were able to get Dr. Hansen, Director of NASA/GISS, to participate as an ACRIM III Co-Investigator. Columbia graduate students at GISS will participate in the ACRIM III science investigation.

'Finally, it should be recognized that the PI has had a unique, central, hands-on role of successfully designing, developing, and operating the ACR for almost 30 years. The current EOS/ACRIM program is planned to cover approximately an additional 15 years. It is not at all clear from the present structure of the science team who would (could) replace Dr. Willson should, for whatever reason, such a replacement become necessary.'

JPL has undergone a considerable downsizing during the past decade. In that process they decided not to retain a commitment to this measurement beyond the first EOS 5 year period. While this management view may have changed recently, the opportunity to mentor a continuing professional TSI capability there did not materialize at a crucial time for EOS.

NASA's response to this concern has been to re-compete the second two 5 year EOS TSI observational periods. The successful proposer for the 2nd, Dr. Gary Rottman of the Laboratory for Atmospheric and Space Physics (LASP) of the University of Colorado, will implement his TSIM TSI experiment in mid 2002 to overlap with the ACRIM III. The development of a new center of expertise in this area at LASP should contribute significantly to the continuity of TSI monitoring.

The long term TSI database owes its current 20+-year length to the cross-fertilization and redundancy of multiple TSI observation teams. Care should be taken to retain these aspects of the EOS TSI monitoring program. The TSI observations, while simple compared to other EOS measurements, are crucially important to climate investigations. There is no demonstrated alternative to the deployment of overlapping TSI experiments to conserve database continuity at the required level of precision. To this end, it is crucially important to retain the low cost approach employed by past ACRIM, ERB and ERBE experiments that facilitated redundancy. Attachment of TSIM to the much more complicated and costly SOURCE experiment will endanger the viability of the TSI database by limiting the frequency of deployment and participation by other competitive, but synergistic TSI experiment teams.

‘The scientific value of ACRIM data seems to be experienced a significant amount of time after the data is initially acquired. The PI needs to clearly communicate to the EOS community when the data will be available for scientific consumption and how he will meet that deadline.’

The inherent value of ACRIM results for EOS-type research is in their cumulative, precise, long-term database. Short-term results have been of interest only to solar physicists. ACRIM data has always been readily available to anyone who requested it.

The early ACRIM results preceded the highly organized UARS and EOS data archiving culture. There was no single place where TSI results were systematically kept. Informal archives have always been maintained by the ACRIM projects and by the NOAA Geophysical Data archive.

ACRIM II was a late addition to the UARS mission. Its data processing mode was not folded into the already well developed UARS CDHF system which was a prototype of the EOSDIS. ACRIM II data is processed under conditions similar to the EOS SIPS modality. ACRIM II results have been archived at both the GSFC and LaRC DAAC’s since their inceptions.

The data processing and archiving approach of the ACRIM III experiment has always conformed to the specifications of the EOSDIS. When the opportunity for a SIPS operation became available ACRIM III opted for it because the approach was more compatible with ACRIM III’s mode of a low cost flight experiment of opportuniuty in the EOS program. The schedule for availability of the data from ACRIM III is addressed in the table above.

‘One possible solution to the data release problem is to employ a DAAC to generate the irradiance product following submissions by the PI of the appropriate calibration coefficients and algorithms.’

This issue has been resolved by adoption of the SIPS mode for ACRIM III.

‘As a general FYI comment, during the ACRIM presentation it was stated that an order of magnitude improvement in the accuracy of the irradiance data could be achieved by flying a cryogenic system on-orbit. A 3 cavity, mechanically cooled cryogenic radiometer for measuring TSI is being developed by a partnership of NPL/UK and AEA Technology. Moreover, this instrument is being studied for possible deployment as an external payload on the International Space Station (ISS). This instrument is briefly discussed in ORM News, Issue 2, Autumn 1996 on page 5.’

I was familiar with this development at the time of the review. One of the device’s original developer’s, John Martin, had expressed an interest in flying a version of their original NPL laboratory 4 Kelvin instrument. I remain unconvinced that this relatively difficult technology will add significantly to a well implemented ‘overlap strategy’ approach to sustaining the long-term TSI database. The cost of a mechanically cooled 4 Kelvin TSI instruments would fund an entire series of ambient temperature TSI radiometer experiments. Further, the ‘overlap strategy’ can produce higher long term precision (< 50 ppm) than the 4 K radiometer, and with much higher reliability.

‘The possibility that there will not be overlap with prior missions is a definite concern. The ACRIM team should also make use of TSI observations from other international missions, if these should become available. ’

Fortunately both the UARS/ACRIM III and SOHO/VIRGO TSI monitors are still operational. At this time we expect to get a substantial overlap comparisons with both and ACRIM III.

6.0 References

Abbot, C.G., Fowle, F.E., (1908) Annals of the Astrophysical Observatory of the Smithsonian Institution, v. 1

Barkstrom, B.R., Harrison, E.F., Lee, R.B., (1990) Trans. Am. Geophys. Union, v. 71, 9, p. 279

Beer, J., Raisbeck, G.M., Yiou, F., (1991), The variation of ^{10}Be and solar activity, The Sun in Time, Ed. Sonnet, C.P., Giampapa, M.S., Mathews, M.S., U. of Arizona Press, pp. 343,359

Brusa, R.W., Frohlich, C., (1972) Entwicklung eines neuen absolutradiometers, Technical Note 1., World Radiation Center, Davos, Switzerland

Chapman, G.A., A.D. Herzog, J.K. Lawrence, (1986) Time integrated energy budget of a solar activity complex, Nature, v. 76, pp 211-219

Chapman, G.A., (1983) 'Ground-based measurements of solar irradiance variations', in "Solar Irradiance Variations on Active Region Timescales", Pasadena, CA, June, 1983, NASA Conference Publication 2310, pp. 73-89

Damon, P.E., Sonnet, C.P., Solar and terrestrial components of the atmospheric ^{14}C variation spectrum, The Sun in Time, Ed. Sonnet, C.P., Giampapa, M.S., Mathews, M.S., U. of Arizona Press, pp. 360,388

Eddy, J. A., (1976) The Maunder Minimum, Science, v. 192, pp. 1189-1202

Foukal, P.A., Lean, J.L.(1988) Magnetic modulation of solar luminosity by photospheric activity, Astrophys. J., v. 328, 347

Foukal, PA.., Lean, (1990) An empirical model of total solar irradiance variation between 1874 and 1988, J. Science, v. 246, 556- 558

Frohlich, C., Pap, J., (1989) A&A, v. 220, 272

Frohlich,C., Delache, P., (1984) 'Solar gravity modes from ACRIM/SMM irradiance data', in Solar Seismology from Space,, ed. by R.K.

Hayley, F., (1964) A rapid response blackbody cavity radiometer, JPL New Technology Rpt. 30-521, Jet Propulsion Laboratory, Pasadena, CA, 91109

Hays, J.D., Imbrie, J., Shackleton, N.J., (1976) Variations in the earth's orbit: pacemaker of the ice ages, Science, v. 194, pp. 1121-1132

Hickey, J.R., Stowe, L.L., Jacobowitz, H., Pellegrino, P. ,Maschoff, R.H., House, F., Vonder Haar, T.H., (1980) Initial determinations from Nimbus 7 cavity radiometer measurements, Science, 208 , p. 281

Hickey, J.R., Alton, B.M., Griffin, F.J., Jacobowitz, H., Pellegrino, P., Smith, E.A, Vonder Haar, T.H., Maschoff, R.H., (1982) J. Solar Energy, v.29, p.125

Hickey, J.R., Griffin, F.J., Jacobowitz, H., Stowe, L., Pellegrino, P., Maschoff, R.H., (1977) EOS (Weekly Pub. of American Geophysical Union), v. 61, p. 355

Hoyt, D., Kyle, L., 'An alternative derivation of the Nimbus7 total solar irradiance variations', Proc. Climate Impact of Solar Variability, NASA Conf. Rpt. 3086 (1990)

Hoyt, D.V., Eddy, J.A., (1982) 'An atlas of variations in the solar constant caused by sunspot blocking and facular emissions from 1874 to 1981', NCAR Tech. Note, National Center for Atmospheric Research/TN 194 + STR

Hudson, H.S., Silva, S., Woodard, M., Willson, R.C., (1982) Solar Physics, v. 76, p.211

Hudson, H.S., Willson, R.C., (1982) Sunspots and solar variability, in The Physics of Sunspots, Proc. Conference on Sunspots, Ed. by L. Cram and J. Thomas, Sacramento Peak Observatory, Sunspot, AZ

Kendall, J.M. Sr.; Berdahl, M., (1970) Two blackbody radiometers of high accuracy, J. Appl. Optics, 9, P. 1082

Kendall, J.M., (1968) The JPL standard total radiation absolute radiometer, JPL Tech. Rpt. 32-1263, Jet Propulsion Laboratory, Pasadena, CA, 91109

Kyle, H.L., Hoyt, D.V., Hickey, J.R., Maschoff, R.H., Vallette, G.J., (1993) Nimbus7 Earth Radiation Budget Calibration History - Part I: The solar channels, NASA Reference Publication 1316

Lean, J. A., Skumanich, White, O. R., (1992) Estimating the sun's radiative -

Lean, J., White, O.R., Livingston, W.C., Heath, D.F., Donnely, R.F., Skumanich,

flux: -

Lee III, R.B., Gibson, M.A., Wilson, R.S., Thomas, S. (1995) Long-term total solar irradiance variability during sunspot cycle 22, JGR, v. 100, pp 1667-1675

Plamondon, J. A., Kendall, J. M., (1965) A cavity type, total radiation radiometer, JPL Space Programs Summary 37-35, v. 4, Jet Propulsion Laboratory, Pasadena, CA, 91109

Plamondon, J.A., (1969) TCFM Solar Observations on Mariner 69, JPL Space Programs Summary, v. 3, p. 162, Jet Propulsion Laboratory, Pasadena, CA, USA

Schatten,K, Miller,N., Sofia, S., Endal, A., Chapman, G.A., (1985) Ap.J., 294, pp 689-696

Solar Influences on Global Change, (1994) Lean, J, Baker, D., , M., Potemra, T., Ried, G., Rind, D., Roble, R., White, O., Williams, D., Willson, R., Withbroe, G., Wuebbles, D., National Academy Press, p. 31

Willson, R.C., J.R. Hickey, (1977), 1976 rocket measurements of the solar constant and their implications for variation in the solar output in cycle 20, The Solar Output and Its Variation, Ed. by O.R. White, Colorado Associated University Press, Boulder, CO, USA, 1977

Willson, R.C., (1980) Solar irradiance observations from the SMM/ACRIM experiment, American Geophysical Union, Toronto, Canada, May

Willson, R.C., Gulkis, S., Janssen, M., Hudson, H.S., Chapman,G.A., (1981), Observations of solar irradiance variability, Science, v.211, p. 700

Willson, R.C., Hudson,H.S., (1981) Astrph. J. Lett., v. 24, p. 185

Willson, R.C., (1982) J. Geoph. Res., v. 86, P. 4319

Willson, R.C., (1984) Measurements of solar total irradiance and it variability, Space Science Reviews, v. 38, pp 203-242

Willson, R.C., Hudson, H.S., Frohlich, C., Brusa, R.W.; (1986) Science, v. 234, p 1114

Willson, R.C., Hudson, H.S., (1988) Nature, v. 332, No. 6167, 810

Willson, R.C., Hudson, H.S., (1991) Nature, v. 351, pp. 42-44

Willson, R.C., Total solar irradiance trend during solar cycles 21 and 22, Science v. 277, 1963-65, 1997

Willson, R.C., Alexander V. Mordvinov, Time-frequency analysis of total solar irradiance variations, JGRL 26, No. 24, pp. 3613-3616, 1999

Woodard, M., Hudson, H., (1983), Nature, v. 305, p.589

Woodard,M., (1984) 'Short-Period Oscillations in the Total Solar Irradiance', Thesis, U. Calif. at San Diego, La Jolla, CA.

Woodard,M., and R. Noyes, (1985) Nature, v. 318, p. 449